

The HELMOD Model in the Works for Inner and Outer Heliosphere: from AMS to Voyager Probes Observations.

M. J. Boschini^{a,b}, S. Della Torre^a, M. Gervasi^{a,c}, G. La Vacca^{a,c}, P. G. Rancoita^{a,*}

^a*INFN sez. Milano-Bicocca, Piazza della Scienza, 3 - 20126 Milano (Italy)*

^b*also CINECA, Segrate, Milano, Italy*

^c*also Physics Department, University of Milano-Bicocca, Piazza della Scienza, 3 - 20126 Milano (Italy)*

Abstract

HELMOD is a Monte Carlo code developed to describe the transport of Galactic Cosmic Rays (GCRs) through the heliosphere from the interstellar space to the Earth. In the current HELMOD version 4 the modulation process, based on Parker's equation, is applied to the propagation of GCRs in the inner and outer heliosphere, i.e., including the heliosheath. HELMOD was proved to reproduce protons, nuclei and electrons cosmic rays spectra observed during solar cycles 23-24 by several detectors, for instance, PAMELA, BESS and AMS-02. In particular, the unprecedented accuracy of AMS-02 observations allowed one a better tuning of the description regarding the solar modulation mechanisms implemented in HELMOD. In addition, HELMOD demonstrated to be capable of reproducing the fluxes observed by the Voyager probes in the inner and outer regions of heliosphere up to its border.

Keywords: Solar modulation, Interplanetary space, Cosmic rays propagation, Termination Shock, heliosphere

1. Introduction

The increased performances of space-borne spectrometers enhanced the accuracy of observed modulated omnidirectional Galactic Cosmic Rays (GCRs) spectral intensity. Furthermore, Voyager probes provided the first and direct observations of Termination Shock and Heliopause. This effort leads to a better capability a) to unveil local interstellar spectra (LIS) of GCR species (e.g., see Boschini et al., 2017, 2018b,c, and references therein), b) to investigate their generation, acceleration and diffusion process within the Milky Way (e.g., see Boella et al., 1998; Strong et al., 2007; Evoli et al., 2008; Putze et al., 2009), and, in turn, c) to possibly untangle features related to new physics – i.e., due to dark matter (e.g., see Bottino et al., 1998; Cirelli and Cline, 2010; Ibarra et al., 2010; Salati, 2011; Weniger, 2011, and references therein) – or to additional astrophysical sources so far not taken into account (e.g., see Chang et al., 2008; Abdo et al., 2009; Adriani et al., 2009a; Cernuda, 2011; Mertsch and Sarkar, 2011; Della Torre et al., 2015; Rozza et al., 2015, and references therein).

A deep understanding of the solar modulation effect – i.e. the physical process affecting GCRs transport in the heliosphere – is needed for the investigations described above. It can be obtained by systematic studies of GCRs spectra observed during different phases of solar activity

by experiments operated on stratospheric balloons (for instance, see Webber and Yushak, 1983; Boezio et al., 1999; Menn et al., 2000; Haino et al., 2004; Shikaze et al., 2007; Abe et al., 2008, 2016) or in space-borne missions (e.g., see Webber and Yushak, 1983; Müller-Mellin et al., 1995; Alcaraz et al., 2000d,c,a,b; Aguilar et al., 2002, 2007; Adriani et al., 2009a,b, 2010, 2011, 2013; Aguilar et al., 2014b, 2015a,b, 2016; Aguilar et al., 2016, 2017, 2018a,b,c,d; Kuznetsov et al., 2017, and reference therein).

Among space missions currently detecting GCRs, AMS-02 – on-board of the International Space Station since May 2011 – observed GCRs flux during the maximum of solar cycle 24, providing data with unprecedented measurement accuracy (Aguilar et al., 2018a,d). On the other hand, Ulysses made unique measurements in the inner part of heliosphere observing particle radiation outside the ecliptic plane (e.g., see Simpson et al., 1992; Simpson et al., 1996; Heber et al., 1996; Ferrando et al., 1996). Among its achievements, it reveals the presence of latitudinal particle intensity gradients whose magnitude depends on solar magnetic field polarity (De Simone et al., 2011; Gieseler and Heber, 2016). Besides, Voyager probes explored heliosphere up to its boundary (and beyond) and showed the truly un-modulated Local Interstellar Spectrum (LIS) of GCRs (McDonald and Lal, 1986; Cummings et al., 1987; Venkatesan and Badruddin, 1990; Zeldovich et al., 2005; Krimigis et al., 2013; Decker et al., 2005; Decker et al., 2008; Stone et al., 2005, 2013; Webber and McDonald, 2013). High precision AMS-02 experimental spectra, together with observations from Ulysses spacecraft outside the ecliptic plane and from Voyager probes up to the he-

*Corresponding author

Email address: piergiorgio.rancoita@mib.infn.it
(P. G. Rancoita)

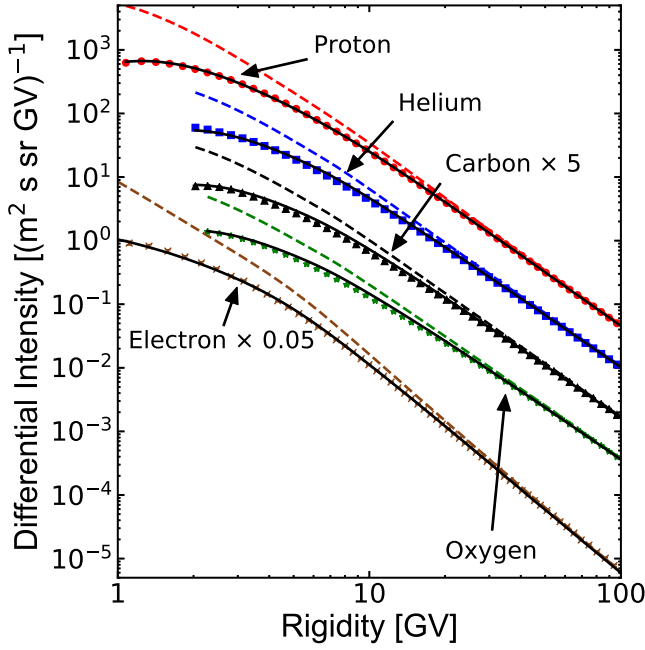


Figure 1: Summary of LISs (dashed line) obtained by means of HELMOD-GALPROP iterative procedure as reported in [Boschini et al. \(2017, for protons\)](#), [Boschini et al. \(2018b, for helium, carbon and oxygen nuclei\)](#), and [Boschini et al. \(2018c, for electrons\)](#). The corresponding modulated spectra (solid lines) obtained using previous HELMOD version 3 are shown with AMS-02 measurements (points) reported in [Aguilar et al. \(2014b, for electron\)](#), [Aguilar et al. \(2015b, for Proton\)](#), and [Aguilar et al. \(2017, Helium, Carbon and Oxygen\)](#).

liosphere boundary, represent a challenge for any modulation model. Finally, it is worth to remark that these data may, in addition, allow a better understanding of space radiation environment close to Earth, thus extending our capability to predict radiation hazards for astronauts and device damages in space missions (e.g., see [Leroy and Rancoita, 2007](#); [Golge et al., 2015](#), and Chapters 7 and 8 of [Leroy and Rancoita 2015](#)).

In this work we present the version 4.0 of HELiospheric MODulation (HELMOD) model currently employed to solve the transport-equation for GCR propagation through the heliosphere down to Earth ([Gervasi et al., 1999](#); [Bobik et al., 2012, 2013](#); [Boschini et al., 2018a](#)). With respect to the previous code version ([Boschini et al., 2018a](#)), the present model improved the accuracy of particle transport mechanisms during solar maxima as described in Sect. 2 and 6. The inclusion of a time dependent heliosphere boundary and of the heliosheath region (Sect. 3) results in an enhanced modulation occurring at low energies and, thus, it required a re-tuning of modulation parameters as described in Sect. 6.

2. Heliospheric Propagation of Cosmic Rays

The particle transport through the heliosphere is a combination of several processes globally described by the Parker

Equation ([Parker, 1965](#), see, e.g., the discussion in [Bobik et al. 2012](#); [Boschini et al. 2018a](#) and reference therein):

$$\frac{\partial U}{\partial t} = \frac{\partial}{\partial x_i} \left(K_{ij}^S \frac{\partial U}{\partial x_j} \right) + \frac{1}{3} \frac{\partial V_{sw,i}}{\partial x_i} \frac{\partial}{\partial T} (\alpha_{rel} T U) - \frac{\partial}{\partial x_i} [(V_{sw,i} + v_{d,i}) U], \quad (1)$$

where U is the number density of GCR particles per unit of kinetic energy T (GeV/nucleon), t is time, $V_{sw,i}$ is the solar wind (SW) velocity along the axis x_i , K_{ij}^S is the symmetric part of the diffusion tensor, $v_{d,i}$ is the particle magnetic drift velocity (related to the anti-symmetric part of the diffusion tensor), and $\alpha_{rel} = \frac{T+2m_r c^2}{T+m_r c^2}$, with m_r the particle rest mass per nucleon in units of GeV/nucleon. The terms in the Parker Equation describe: (i) the diffusion of GCRs scattered by magnetic irregularities, (ii) the adiabatic energy losses/gains due to the propagation in the expanding magnetic fields carried in the SW, (iii) an effective convection resulting from the SW convection with velocity \vec{V}_{sw} , and (iv) the magnetic drift effects related to the drift velocity (\vec{v}_d). Overall, the heliospheric modulation results in energy losses and suppression of the fluxes of CR species compared to the LIS. These effects are controlled by the level of solar activity, by the solar magnetic field polarity, and are energy- and charge-sign-dependent.

It is widely accepted that K^S components parallel to the magnetic field ($K_{||}$) are larger than perpendicular components ($K_{\perp,i}$), and should be described using non-linear theories (for a review see, e.g., [Shalchi, 2009](#)). At high rigidities (i.e., $\gg 1$ GV) the diffusion tensor should have a linear (or quasi-linear) rigidity dependence (e.g., see [Gloeckler and Jokipii, 1966](#); [Gleeson and Axford, 1968](#); [Jokipii, 1966, 1971](#); [Perko, 1987](#); [Potgieter and Le Roux, 1994](#); [Strauss et al., 2011](#)). The transition from the quasi-linear to the non-linear regimes results in a “flattening” of rigidity dependence at low values as observed, for instance, by [Palmer \(1982\)](#) and [Bieber et al. \(1994\)](#). In the present work we use a functional form with a rigidity dependence following the one presented in [Boschini et al. \(2018a, and reference therein\)](#):

$$K_{||} = \frac{\beta}{3} K_0 \left(\frac{P}{1 \text{ GV}} + g_{low} \right) \left(R_c + \frac{R}{1 \text{ AU}} \right), \quad (2)$$

where K_0 is the diffusion parameter, which depends on the solar activity and magnetic polarity, β is the particle speed in units of the speed of light, $P = qc/|Z|e$ is the particle rigidity in GV, R is the heliocentric distance from the Sun in AU, and, finally, g_{low} (discussed in [Boschini et al., 2018a](#)) and R_c are parameters tuned to describe radial GCR intensity gradients on the inner heliosphere (see Sect. 6).

The diffusion parameter K_0 fixes the normalization of $K_{||}$. It changes with time as defined by equation (6–7) of [Boschini et al. \(2018a, and references therein\)](#). In turn, as introduced in [Boschini et al. \(2018c\)](#), the diffusion parameter K_0 includes a correction factor that re-scales the

absolute value of K_{\parallel} to account for the drift contribution. This correction factor (discussed in Sect. 6) is evaluated using the proton flux during the period of positive polarity of the Heliospheric Magnetic Field (HMF) and applied to both electrons and ions when the condition $qA > 0$ occurs; an additional correction has to be evaluated using electron flux and applied to negative-charged particle diffusion during positive HMF polarity period ($A > 0$).

The perpendicular diffusion coefficient is taken to be proportional to K_{\parallel} with a ratio $K_{\perp,i}/K_{\parallel} = \rho_i$ for both R and θ i -coordinates (e.g., see Potgieter, 2000; Burger and Hattingh, 1998a, and references therein). At high rigidities, this description is consistent with quasi-linear theories (QLTs). Palmer (1982) constrains the value of ρ_i between 0.02 and 0.08 at Earth. In the current version of the model, we found $\rho_i \approx 0.065$ for protons and ions and $\rho_i \approx 0.05$ for electrons and positrons. The slight difference between ρ_i values might be related to the mass differences between massive particles (i.e, protons and nuclei) and leptons (i.e electron and positrons). As discussed in Bobik et al. (2012), we used an enhanced $K_{\perp,\theta}$ by a factor 2 in the polar regions in order to reproduce the amplitude and rigidity dependence of the latitudinal gradients of GCR differential intensities for protons (see Section 5.4 of Boschini et al., 2018a, and reference therein).

As also remarked in Bobik et al. (2013), in this description K_{\parallel} has a radial dependence $\propto R$ but no latitudinal dependence; nevertheless, the reference frame transformations from the field-aligned frame to the spherical heliocentric one (see, e.g., Burger et al., 2008) introduce a dependence on the polar angle. As was shown in Bobik et al. (2013), this is enough to explain the latitudinal gradient observed by Ulysses during the latitudinal *fast scan* in 1995 (see e.g. Heber et al., 1996; Simpson et al., 1996).

We use the drift model originally developed by Potgieter and Moraal (1985) – that includes description of *regular drift* due to large scale structure of heliospheric magnetic field, and the *neutral sheet drift* described, e.g, in Jokipii and Thomas (1981); Hattingh and Burger (1995) –, and refined using Parker’s magnetic field with polar corrections as reported in Bobik et al. (2013) (see also Raath et al., 2016, for a discussion about modified Parker’s magnetic field). Previous works underlined the importance of additional drift suppression during high activity periods (see, e.g., discussion in Ferreira and Potgieter, 2004; Bobik et al., 2013). This is due to the presence of turbulences in the interplanetary medium reducing the global effect of CR drift in the heliosphere (Engelbrecht et al., 2017). In the present work we extend this description including a time dependent *drift suppression factor* related to solar activity as discussed in Sect. 6.

LIS spectra are assumed to be nearly isotropic at the heliosphere boundary due to the relative small dimension of the heliosphere (~ 100 astronomical units) compared with the expected cosmic-ray density gradient scale in the galaxy (~ 18 pc) (see, e.g., discussion in Zhang et al., 2015). As described by Boschini et al. (2017), in order to

derive the physically motivated LIS of GCR species, an iterative procedure was developed to feed the GALPROP output into HELMOD to compare with AMS-02 data as observational constraints (Masi, 2016). The main propagation parameters were treated as free parameters in the scan using GALPROP (Strong and Moskalenko, 1998; Moskalenko and Strong, 1998). The parameters defining the injection spectra, such as spectral indices and the break rigidities, were also treated as free parameters, but their exact values, below ~ 50 GV, depend on the solar modulation. As a matter of fact, the low energy part of the spectra is tuned together with the solar modulation parameters. LIS parametrization is mainly constrained by measurements from Voyager probes (Cummings et al., 2016), at low energy, and AMS-02 (Aguilar et al., 2014a,b, 2015a,b, 2016; Aguilar et al., 2016, 2017), at high energy.

In Fig. 1 we summarize the LISs obtained by means of HELMOD-GALPROP iterative procedure as reported in Boschini et al. (2017, for protons), Boschini et al. (2018b, for helium, carbon and oxygen nuclei), and Boschini et al. (2018c, for electrons); the corresponding HELMOD modulated spectra obtained using previous HELMOD version 3 is shown with AMS-02 measurements reported in Aguilar et al. (2014b, for electron), Aguilar et al. (2015b, for proton), and Aguilar et al. (2017, for helium, carbon and oxygen nuclei).

3. The HelMod Heliosphere

The boundary of the heliosphere, called heliopause (HP), is a contact discontinuity separating the solar cavity – in which the SW plasma is flowing – from the interstellar space. It also represents the extreme limit beyond which solar modulation does not affect CR flux. Thus, outside HP the truly pristine LIS of GCR spectra could be observed.

After being accelerated in the solar corona (Parker, 1958) SW adiabatically expands in radial direction with supersonic speed. In its journey towards the external regions of the heliosphere SW flow changes its supersonic regime, through the formation of a physical boundary called Termination Shock (TS) which, in practice, separates the inner part of the heliosphere¹ from the outer region², also known as heliosheath (HS).

The heliosphere boundaries (i.e., TS and HP) were extensively discussed in the literature (e.g., Parker, 1961, 1963; Axford, 1972; Holzer, 1989; Zank, 1999, 2015 and references therein). Recently, fundamental advancements in the knowledge of the outer heliosphere were achieved

¹The inner part of the heliosphere – corresponding to the space region from the Sun up to the TS – will be indicated as inner heliosphere in the following.

²The outer part of the heliosphere – corresponding to the space region from the TS up to the HP – will be indicated as outer heliosphere in the following.

by means of both Voyager probes, which provided on-site observations of TS and HP positions, SW plasma and magnetic field properties (e.g., see [Richardson et al., 2008](#); [Richardson, 2013](#); [Richardson and Decker, 2015](#); [Burlaga and Ness, 2016](#); [NASA-OMNIweb, 2018](#)). In Parker’s model of the heliosphere ([Parker, 1961, 1963](#)), such pieces of information can be exploited for allowing us to estimate the time dependence of both TS and HP positions – i.e., those currently used in HELMOD –, as discussed in Sect. 4. For instance, the predicted TS values are in good agreement with those observed: for Voyager 1 (Voyager 2) the detected TS position is 93.8 AU (83.6 AU) and the predicted is 91.8 AU (86.3 AU), i.e. within 3 AU; and, using the HP position observed by Voyager 1, the predicted value is 120.7 AU at the time of the Voyager 2 HP crossing which occurred at 119 AU. Furthermore, the interstellar magnetic field strength measured by Voyager 1 is $(0.48 \pm 0.04)\text{nT}$ ([Burlaga and Ness, 2016](#)). In the context of the Parker model, at the TS positions observed by Voyager 1 and Voyager 2, such a magnitude requires that the value of the dimensionless stagnation pressure ([Parker, 1963](#)) approaches its maximum value, i.e., the one allowed for a spherical diamagnetic solar cavity (see discussion in Sect. 4). It should be remarked that, from the measurements of energetic neutral atoms by IBEX ([McComas et al., 2009](#)) and Cassini ([Krimigis et al., 2009](#)), [Dialynas et al. \(2017\)](#) strongly suggested a diamagnetic bubble-like heliosphere³ with negligibly small tail-like features (see also [Drake et al., 2015](#); [Opher et al., 2015, 2017](#)).

In HelMod model, so far the inner region of the heliosphere was described as an *effective heliosphere* ([Bobik et al., 2012](#)) with a radius – i.e., an effective TS distance – of 100AU. Solar modulation was, then, treated by subdividing it in 15 radially equally-spaced regions. Each i -th region traveled by CR particles is characterized by heliospheric parameters evaluated at i -Carrington rotations back-in-time, corresponding to the time needed by SW for reaching it ([Bobik et al., 2012](#); [Boschini et al., 2018a](#)). The actual dimensions of the heliosphere are accounted for by scaling the position of TS by the time dependent values obtained as described in Sect. 4. The HS is included as a single additional region on top of the 15 inner regions with its actual size as calculated in Sect. 4. As discussed in Sect. 4 the TS and HP latitudinal profile in the nose region was determined taking into account the latitudinal variation of the ISM ram pressure component of the total pressure on the HP surface. In the anti-nose region only the magnetic and plasma pressure were accounted for. As a consequence, an asymmetry in the direction of the ISM flow is introduced (see Fig. 3 in Section 4). Finally a cylindrical symmetry with respect to the axis along the sun-nose direction was applied to have full three-dimensional

heliospheric boundaries.

4. Heliospheric boundaries in HelMod: time dependent Termination Shock and Heliopause

The analytical modelization of the heliosphere dates back to [Parker \(1961\)](#) (see also discussions in [Parker, 1963](#)). In the framework of Parker’s model the position of the termination shock (TS) is obtained from hydro-dynamical considerations. The main hypothesis is that the heliopause (HP) is a contact discontinuity (e.g., see [Suess, 1990](#)) separating the region in which the propagation of the solar wind (SW) dominates from the interstellar medium⁴ (ISM). In such a model, the SW flows along streamlines from the inner part of the heliosphere, passing through the TS and traversing the heliosheath (HS) up to the stagnation point⁵ (with P_{ISM} as stagnation pressure) on the HP in a one-dimensional radial approximation. Assuming a spherical heliocentric geometry, the SW is treated as an ideal gas⁶ with adiabatic index γ expanding steadily, radially and adiabatically towards the TS. Before reaching the TS, the largely dominant contribution to the total SW pressure⁷ is provided by the ram pressure $p_{\text{ram}} = \rho u^2$, where ρ is the plasma density and u the SW speed. Moreover, for a constant SW speed up to the TS ([Parker, 1958](#)) and from the mass conservation, one finds that the plasma density and the pressure p scale with distance as

$$\rho(R) = \rho_{\text{obs}}(R_{\text{obs}}/R)^2, \quad (3)$$

where the subscript *obs* refers to the quantities measured by an observer located at the heliocentric distance R_{obs} .

As discussed in [Parker \(1961\)](#), before reaching the stagnation point, the SW must go through a shock transition: SW plasma abruptly slows down and is compressed, so that density increases⁸. For a shock occurring in a plane perpendicular to the direction of flow⁹ (normal shock) – as discussed for the SW shock by [Parker \(1961, 1963\)](#) –, the hydrodynamical quantities in the neighborhood of the shock are connected by the Rankine-Hugoniot relations (e.g. see §85 chapter 9 in [Landau and Lifshitz, 1959](#))

⁴For instance, after November 5 2018 the plasma instrument on board of Voyager 2 has observed no SW flow in the environment around the spacecraft and this can be possibly considered as an experimental observation that the spacecraft entered into the interstellar space ([NASA’s Voyager team, 2018](#)).

⁵In fluid dynamics, a stagnation point is a point in a flow field where the local velocity of the fluid is zero.

⁶For a mono-atomic gas with three degrees of freedom, the specific heat ratio or adiabatic index is $\gamma = 5/3$.

⁷The interplanetary magnetic field pressure and thermal pressure can be neglected. In fact, their intensities were estimated to be on average two orders of magnitude smaller than the ram pressure from on-site spacecraft measurements ([NASA-OMNIweb, 2018](#)).

⁸The magnetic field after TS increases by about a factor 2 (e.g. see [Burlaga et al., 2008](#)). However, the magnetic pressure is still negligible.

⁹For the SW propagation, the plane is perpendicular to the radial direction.

³Under the condition that there is no interstellar magnetic field, [Parker \(1961, 1963\)](#) discussed the case of a steady subsonic interstellar wind leading to a comet-like shape (see, e.g., [Axford, 1972](#); [Holzer, 1989](#); [Zank, 1999, 2015](#), and references therein).

which in the *strong* shock limit (*i.e.*, for high Mach numbers) allow one to provide, for instance, the relationship between particle density, SW velocity and ram pressure at TS, immediately before and immediately after the shock occurrence:

$$p_{ram\ 2TS} = \rho_{2TS} u_{2TS}^2 \quad (4)$$

$$= \frac{\gamma - 1}{\gamma + 1} p_{ram\ 1TS}; \quad (5)$$

in the above expressions (and in the following) subscript 1TS (2TS) refers to quantities just before the TS occurs (just after the TS has occurred).

The Parker hypothesis of *strong* shock proved to be a fairly good approximation also in light of the on-site plasma measurements by Voyager 2 probe. In fact, the Mach number can be estimated using temperature and SW speed; one finds that its value is about 9 (Richardson et al., 2008) just before the TS (*i.e.*, at 83.6 AU) using the data from Voyager 2 (NASA-OMNIweb, 2018). Furthermore, using the same source of data, the mean ram pressure calculated in the 2 AU before reaching the TS zone¹⁰ located at 83.6 AU is 3.26×10^{-4} nPa, while in the 2 AU after the TS zone is 0.83×10^{-4} nPa. Therefore their ratio is about 3.9 and it is in agreement with the value 4 – expected for a strong shock of a monoatomic gas (*e.g.*, see Eq. (5)) – which, in the Parker model, provides the ratio of 1/7~14.3% (*e.g.*, see Parker, 1961) between kinetic pressure¹¹ and the stagnation pressure¹².

In addition, although the SW speed in the HS does not exhibit an appreciable dependence on R (Richardson, 2013), in the region downstream the TS, its radial component ($V_{sw,2R}$) progressively slows down flowing in the HS towards the stagnation point (Langner et al., 2003; Richardson and Decker, 2015). In Fig. 2, the radial SW speed (full circle) is obtained with a coordinate transformation (*e.g.*, see Burlaga, 1984) from the data in NASA-OMNIweb (2018). Such a decrease is compatible with the $1/R^2$ behavior (the solid line) given by:

$$V_{sw,2R}(R) = u_{2TS} \left(\frac{R_{TS}}{R} \right)^2, \quad (6)$$

where $u_{2TS} = 150.7$ km/s (the SW speed average value calculated in the 2 AU after reaching the TS zone) and $R_{TS} = 83.6$ AU, *i.e.* the position of the TS observed by Voyager 2.

In the Parker model, the TS position is determined as the distance (R_{TS}) at which the total pressure in the

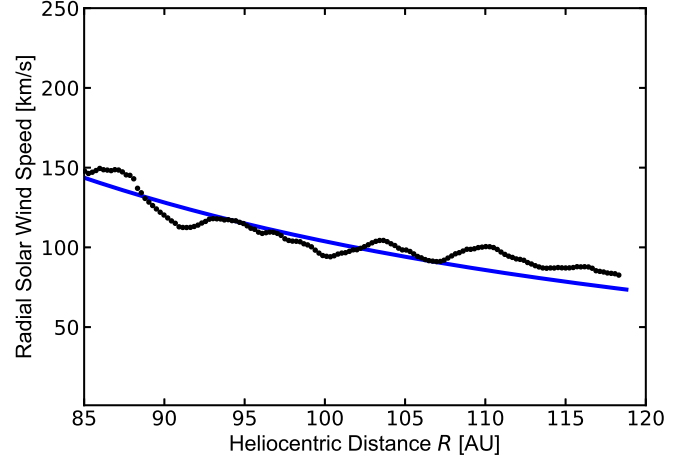


Figure 2: Radial component of the SW speed in the HS ($V_{sw,2r}$) as function of the heliocentric distance R downstream the Voyager 2 TS: the data are obtained with a coordinate transformation (*e.g.*, see Burlaga, 1984) from the data in NASA-OMNIweb (2018); the solid line is the $1/R^2$ behavior (see text).

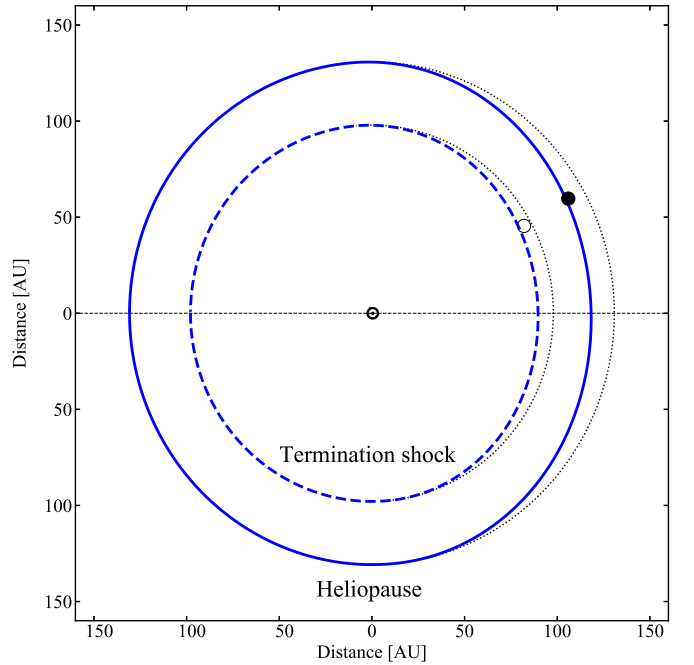


Figure 3: Meridian section of the heliosphere as described in Eq. (15). The dashed (solid) line shows the latitudinal profile of the TS (HP) at the time and HCI latitude of the Voyager 1 TS (HP) crossing. The open (full) circle denotes the instantaneous position of Voyager 1 at TS (HP) crossing.

¹⁰We assume that the TS region extends for 1 AU before and after the TS position determined at 83.6 AU by Voyager 2.

¹¹The kinetic pressure corresponds to $p_{kin} = \frac{1}{2} \rho u^2$.

¹²For Voyager 2 at the TS the ratio between kinetic pressure ($\frac{1}{2} 0.83 \times 10^{-4}$ nPa) and the interstellar pressure (2.62×10^{-4} nPa, as discussed later) is about 15.8%. In general, after the shock, the thermal pressure due to ionized and neutral particles (*e.g.*, see discussion in Richardson et al., 2008) becomes dominant with a value determined by P_{ISM} , as well as the ratio between kinetic and thermal pressure.

Table 1: Physical parameters of the local interstellar medium used in this work.

	Parameter	Value	Reference
v_{ISM}	Speed	26 km/s ⁻¹	Möbius, E. et al. (2004) Bzowski et al. (2015)
n_{ISM}	Proton number density	0.07 cm ⁻³	Slavin, J. D. and Frisch, P. C. (2008) Möbius, E. et al. (2004)
T_{ISM}	Temperature	7000 K	Bzowski et al. (2015)
B_{ISM}	ISMF strength	0.50 nT	(see discussion in the text)

region downstream the shock is equal to the ISM stagnation pressure P_{ISM} . Parker (1961) derived two expressions for the TS position depending on whether the expansion of the shocked SW in the HS occurs through an *isentropic* (i.e., reversible adiabatic) or an *incompressible* expansion. Numerically the relative difference between those two approaches is less than 0.4% for a monatomic gas; for an incompressible flow (i.e., with plasma density $\rho = \text{const}$) one finds that the expression for R_{TS} is given by:

$$R_{TS} = R_{\text{obs}} \left(\frac{\rho_{\text{obs}} u_{\text{obs}}^2}{P_{\text{ISM}}} \right)^{\frac{1}{2}} \left[\frac{\gamma + 3}{2(\gamma + 1)} \right]^{\frac{1}{2}}. \quad (7)$$

It has to be remarked that the P_{ISM} determines the physical conditions for which the shock occurs at R_{TS} , i.e., the inner boundary of the HS. In general, in the HS, the hydrodynamical quantities and its boundaries (TS and HP) are related to P_{ISM} . Voyager 1 has provided the first on-site observation of HP position (121.6 AU on Aug 2012) which allows one to determine, for instance, the value of the outward radial ram pressure of the SW at the outer heliospheric boundary.

In the Eq. (7), the SW ram pressure depends on the solar activity, while P_{ISM} (discussed later) is commonly assumed to be time independent. Therefore, R_{TS} can be determined as function of time using the monthly averages of the SW plasma parameters measured by various satellites (e.g., Voyager 2, Wind, ACE, Ulysses) along the last 60 years (NASA-OMNIweb, 2018; UFA, 2018). The mean value of those monthly averages finally provides the monthly estimate of R_{TS} ¹³ (currently used in HELMOD). In Eq. (7) the values of ρ_{obs} and u_{obs} are found taking into account the time lag (Δt_{TS}) needed to the SW to travel from the observation point at R_{obs} to R_{TS} , i.e.,

$$\Delta t_{TS} = \int_{R_{\text{obs}}}^{R_{TS}} \frac{dR}{V_{\text{sw}}(R)}, \quad (8)$$

$$= \frac{R_{TS} - R_{\text{obs}}}{u_{\text{obs}}}, \quad (9)$$

where Eq. (9) is employed for a constant SW speed¹⁴ equal to u_{obs} . It must be remarked that using the out-of-ecliptic

data from Ulysses the computed SW ram pressure apparently does not show a latitudinal dependence. In fact, at high latitudes the SW density decrease is almost completely compensated by the SW speed increase. The so calculated ram pressures are well compatible with those obtained with the data from the other satellites within the monthly fluctuations. Therefore, R_{TS} does not exhibit observable latitudinal dependencies.

The other quantity appearing in Eq. (7) is the stagnation pressure P_{ISM} . As already discussed by Parker (1963) (see also Parker, 1961), to a first approximation P_{ISM} can be estimated by adding the interstellar (IS) magnetic field pressure (p_{mag}), the kinetic pressure due to IS wind (p_{kin}), the thermal pressure of the IS plasma (p_{th}), i.e.,

$$P_{\text{ISM}} = p_{\text{mag}} + p_{\text{kin}} + p_{\text{th}}. \quad (10)$$

The values for p_{kin} , p_{th} and p_{mag} are discussed in the following (e.g. see Eqs. (13, 14, 16)). A lower contribution to P_{ISM} is expected from the CR pressure (p_{CR}). As already discussed by Parker (1963), p_{CR} accounts for the difference between the pressure derived from the CR omnidirectional intensity in the IS space outside the HP with respect to that one obtained by the CR omnidirectional intensity immediately inside the HP. The CR pressure is determined as in Ip and Axford (1985) (see also references therein) integrating the CR particle density $U(T)$ for protons and helium nuclei (these two species constitute the dominant contribution to the overall CR omnidirectional intensity). Their intensities immediately inside the HP are obtained from the modulated HELMOD spectrum in the HS region close to the HP (e.g., see Section 5 and the upper panel of Fig. 6). The value found for p_{CR} is about 2.4×10^{-6} nPa, i.e., it is of the order or lower than 1% of the overall P_{ISM} and can be neglected. The dominant contribution to the stagnation pressure comes from the IS magnetic field pressure (e.g., see equation (9.27) of Parker, 1963):

$$p_{\text{mag}} = \Pi^2 \frac{B_{\text{ISM}}^2}{2\mu_0}, \quad (11)$$

where B_{ISM} is the average IS magnetic field magnitude, μ_0 is the permeability of free space, and $\Pi^2 = 2.25$ is the dimensionless stagnation pressure (see Parker, 1963). In Parker's model, this value is the maximum allowed for Π^2 parameter, and corresponds to an heliosphere described as a spherical "diamagnetic" region of radius l in which the SW is streaming away from it along two opposite channels

¹³On average the standard deviation is about 5.8 AU

¹⁴The typical value of Δt_{TS} amounts to ~ 1 year (15 Carrington rotations) for the SW propagating from 1AU to $R_{TS} \sim 100$ AU with an average speed ~ 450 km/s.

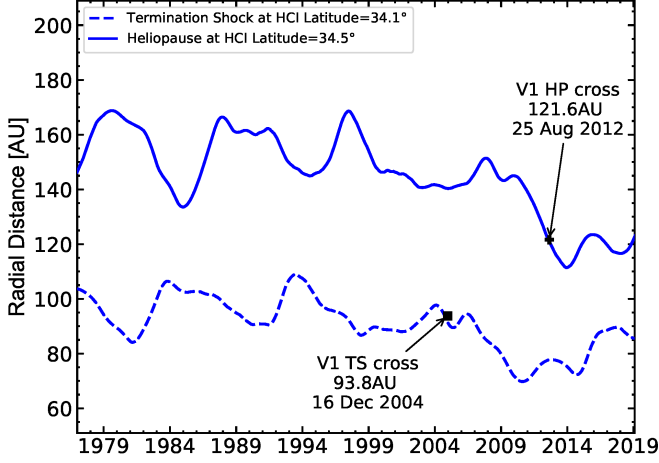


Figure 4: Time variation of monthly averaged position of TS (dashed line) and HP (solid line), calculated from 1977 up to the end of 2018. TS is calculated at HCI-latitude 34.1° , while HP at HCI-latitude 34.5° to match Voyager 1 trajectory. The predicted TS distance at the time of Voyager 1 crossing is 91.8 AU.

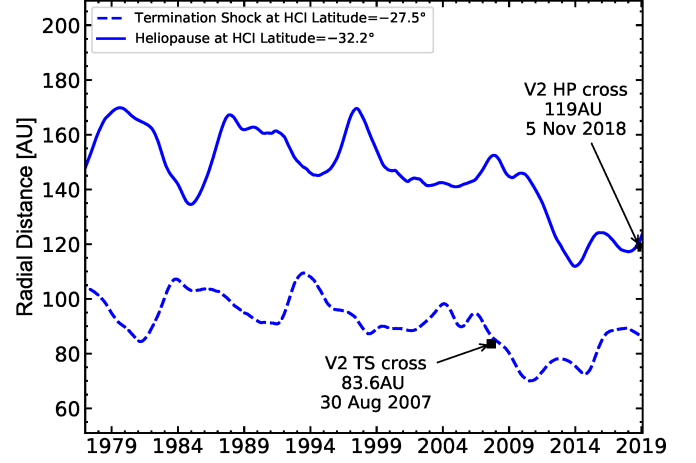


Figure 5: Time variation of monthly averaged position of TS (dashed line) and HP (solid line), calculated from 1977 up to the end of 2018. TS is calculated at heliolatitude -27.5° , while HP at heliolatitude -32.2° to match trajectory of Voyager 2. The predicted TS distance at the time of Voyager 2 crossing is 86.3 AU, while the predicted HP distance at the time of Voyager 2 crossing is 120.7 AU.

of radius $c \rightarrow 0$ along the IS magnetic field direction (e.g., see Figure 9.3 in Parker, 1963). In addition, the radius of the boundary between the IS magnetic field and the SW, i.e. the heliopause, overlaps that one of the “diamagnetic” region. The IS wind pressure (p_{kin}) is due to the relative motion of the heliospheric cavity with respect to the ISM. In the HCI reference system¹⁵ this flow occurs close to the x-axis direction and determines the heliospheric nose direction¹⁶; p_{kin} is given by

$$p_{\text{kin}} = \frac{1}{2} n_{\text{ISM}} m_p [v_{\text{ISM}} \cos(\alpha)]^2, \quad (12)$$

$$= 0.40 \times 10^{-4} \cos^2(\alpha) \text{ nPa}, \quad (13)$$

where n_{ISM} (see Table 1) is the proton number density¹⁷, m_p is the proton mass, v_{ISM} (see Table 1) the relative IS wind speed and, finally, α is the difference between the HCI heliolatitude of the nose and the heliolatitude of the point at which the pressure is calculated. In Eq. (12), $v_{\text{ISM}} \cos(\alpha)$ is the IS velocity component normal to the HP boundary. A further contribution comes from the thermal pressure of the interstellar plasma (p_{th}):

$$\begin{aligned} p_{\text{th}} &= 2 n_{\text{ISM}} k_B T_{\text{ISM}}, \\ &= 0.14 \times 10^{-4} \text{ nPa}, \end{aligned} \quad (14)$$

where k_B is the Boltzmann constant, T_{ISM} (see Table 1) is the ISM temperature and n_{ISM} is its number density;

¹⁵In the Heliocentric Inertial (HCI) reference frame the x-axis is directed along the intersection line of the ecliptic plane and solar equatorial plane. The z-axis is directed perpendicular to and northward of the solar equator plane, and the y-axis completes the right-handed set (e.g., see Burlaga (1984); Fränz and Harper (2002, 2017)).

¹⁶At $[178.3^\circ, 5.1^\circ]$ in the HCI system of reference (Bzowski et al., 2015).

¹⁷The electron contribution to the overall density is negligible because of their small mass with respect to that of the protons.

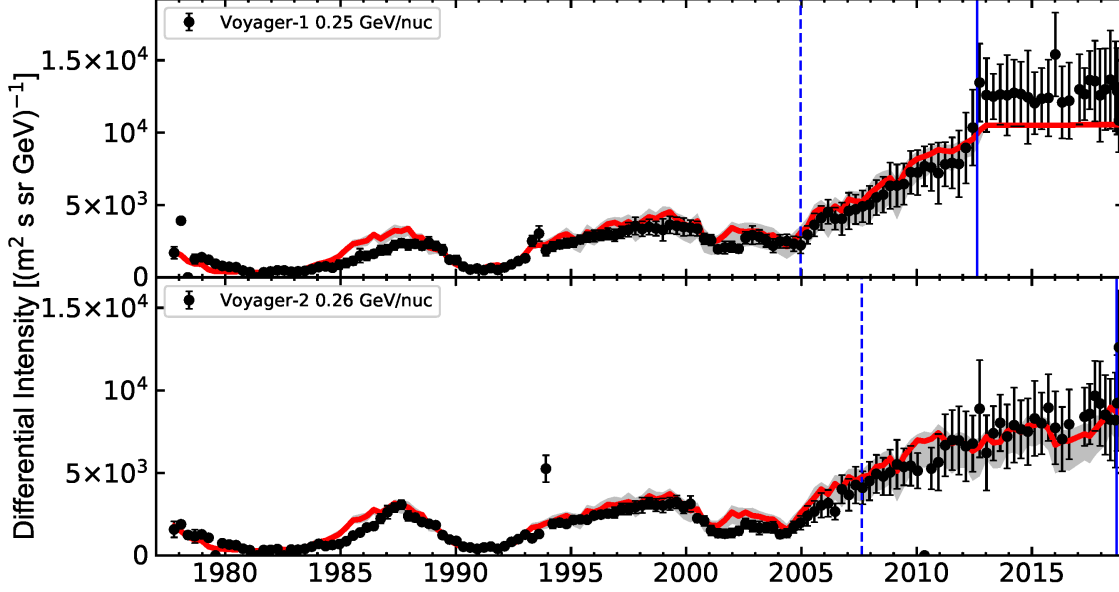
the factor 2 accounts for the equal amount of protons and electrons.

The first on-site observation of R_{TS} at 93.8 AU was provided by Voyager 1 on 16 December 2004. We have to remark that, since R_{TS} depends on the actual value of P_{ISM} (Eq. (10)) whose dominant term is p_{mag} (Eq. (11)), at the date of Voyager 1 crossing we can estimate the value of p_{mag} , then that of B_{ISM} . In fact, B_{ISM} can be derived from Eq. (7) introducing R_{obs} , ρ_{obs} and u_{obs} – obtained back on time (e.g. see Eq. (9)) from Voyager 2, Wind, ACE, Ulysses (also NASA-OMNIweb) –, the thermal pressure $p_{\text{th}} = 0.14 \times 10^{-4} \text{ nPa}$ (Eq. (14)) and the kinetic pressure $p_{\text{kin}} = 0.30 \times 10^{-4} \text{ nPa}$, i.e. calculated at HCI-latitude¹⁸ of 34.1° (Eq. (13)). For $\Pi^2 = 2.25$ (i.e., that allowed for a spherical diamagnetic solar cavity) the average magnetic field needed to get $R_{TS} = 93.8 \text{ AU}$ on 16 December 2004 is $B_{\text{ISM}} = (48.6 \pm 2.0) \times 10^{-2} \text{ nT}$, well in agreement with the value measured by Voyager 1 in the IS space¹⁹, i.e., $(48.0 \pm 4.0) \times 10^{-2} \text{ nT}$ (Burlaga and Ness, 2016). Using the same procedure, for Voyager 2 which crossed the TS at $R_{TS} = 83.6 \text{ AU}$ on 30 August 2007, the kinetic pressure $p_{\text{kin}} = 0.25 \times 10^{-4} \text{ nPa}$, i.e. calculated at HCI-latitude of -27.5° , for $\Pi^2 = 2.25$ the average magnetic field needed to get $R_{TS} = 83.6 \text{ AU}$ on 30 August 2007 is $B_{\text{ISM}} = (51.9 \pm 1.3) \times 10^{-2} \text{ nT}$. As discussed above, P_{ISM} depends on HCI-latitude α (e.g. see Eqs. (10) and (13)), R_{TS} calculated from Eq. (7) has to depend, in turn, on α (e.g., see Fig. 3),

¹⁸It is worth to mention that the Voyager 1 spacecraft is actually traveling in a direction close to the one of the interstellar magnetic field (Frisch et al., 2015; Zirnstein et al., 2016).

¹⁹It should be remarked that the consistency between the calculated and observed TS position for Voyager 1 requires, in turn, the maximum value of the dimensionless stagnation pressure Π^2 .

Figure 6: HELMOD version 4 modulated spectra (red solid line) – obtained using proton LIS from [Boschini et al. \(2017\)](#) – compared with measurements at ~ 0.25 GeV (black points) from instruments on-board of Voyager 1 (upper Panel) and Voyager 2 (lower panel). Voyager’s data are from ([NASA-Voyager, 2018](#)). Vertical dashed line indicates the TS crossing, while vertical solid line reports the HP crossing of Voyager 1.



i.e.,

$$R_{TS}(\alpha) = \begin{cases} R_{TS}(90^\circ) - [R_{TS}(90^\circ) - R_{TS}(0^\circ)] \cos^2(\alpha), & \text{if } |\alpha| < 90^\circ, \\ R_{TS}(90^\circ) & \text{otherwise.} \end{cases} \quad (15)$$

In the nose direction the IS wind affects the extension of the TS by a factor²⁰ not exceeding 10%.

In the present HELMOD model the R_{TS} positions are obtained from Eq. (7) using the mean of the two so derived B_{ISM} values (see Table 1); the corresponding p_{mag} to be used in Eq. (10) becomes:

$$p_{mag} = 2.24 \times 10^{-4} \text{ nPa.} \quad (16)$$

In Fig. 4 (Fig. 5) the time variation of the positions of the TS (dashed line) from 1977 to up to the end of 2018 is shown at 34.1° (-27.5°). By inspecting the two figures, one can remark that the predicted values are in good agreement with those observed: for Voyager 1 (2) the observed TS position is 93.8 AU (83.6 AU) and the predicted is 91.8 AU (86.3 AU), i.e. within 3 AU.

As already discussed, the ram pressure in the radial direction at the HP (as well as that at the TS) depends on P_{ISM} . For the motion of an incompressible fluid reaching the HP at the position R_{HP} , one finds that, independently of the HCI latitude, the ratio (T_H) of the radial ram pressure at the TS with respect to that at the HP using Eqs. (4)

and (6) is

$$T_H = \left(\frac{R_{HP}}{R'_{TS}} \right)^4, \quad (17)$$

where R'_{TS} is the TS position back on time²¹ by Δt_{HP} , i.e., that at which the SW stream was leaving the TS with speed u'_{2TS} . In the current HELMOD model, R'_{TS} are obtained from Eq. (7) using the monthly averages of the SW plasma parameters measured by various satellites, as previously discussed. Thus the HP boundaries²² are described by Eq. (15) by replacing the $R'_{TS}(\alpha)$ with $R_{HP}(\alpha)$ once the ratio T_H is determined using Voyager 1 observations (e.g., see Fig. 3). It should be remarked that, from the measurements of energetic neutral atoms by IBEX ([McComas et al., 2009](#)) and Cassini ([Krimigis et al., 2009](#)), [Dialynas et al. \(2017\)](#) strongly suggested a diamagnetic bubble-like heliosphere²³ with few substantial tail-like features (see also [Drake et al., 2015](#); [Opher et al., 2015, 2017](#)). Δt_{HP} can be computed using Eq. (17) and by introducing the appropriate quantities in Eq. (8); finally, one gets

$$\Delta t_{HP} = \frac{R'_{TS}}{3u'_{2TS}} \left(\sqrt[4]{T_H^3 - 1} \right). \quad (18)$$

Voyager 1 provided the first on-site measurement of R_{HP} (121.6 AU on 25 August 2012). The estimation of

²¹The typical value of Δt_{HP} amounts to ~ 4 years.

²²In the nose direction the interstellar wind affects the extension of the HP by a factor not exceeding 10%.

²³Under the condition that there is no interstellar magnetic field, [Parker \(1961, 1963\)](#) discussed the case of a steady subsonic interstellar wind leading to a comet-like shape (see, e.g., [Axford, 1972](#); [Holzer, 1989](#); [Zank, 1999, 2015](#), and references therein).

²⁰This small compression is not present in [Parker \(1963\)](#), because he discussed the case of a diamagnetic heliospheric cavity in absence of the IS wind.

Figure 7: HELMOD version 4 solutions at 2 GV (red solid line) for protons (top panel), helium nuclei (central panel), and electrons (bottom panel) obtained using the corresponding LISs from [Boschini et al. \(2017\)](#), [Boschini et al. \(2018b\)](#), and [Boschini et al. \(2018c\)](#), respectively. In the same plot, experimental data, at the nearest rigidity bin, from EPHIN, BESS, PAMELA and AMS-02 are reported.

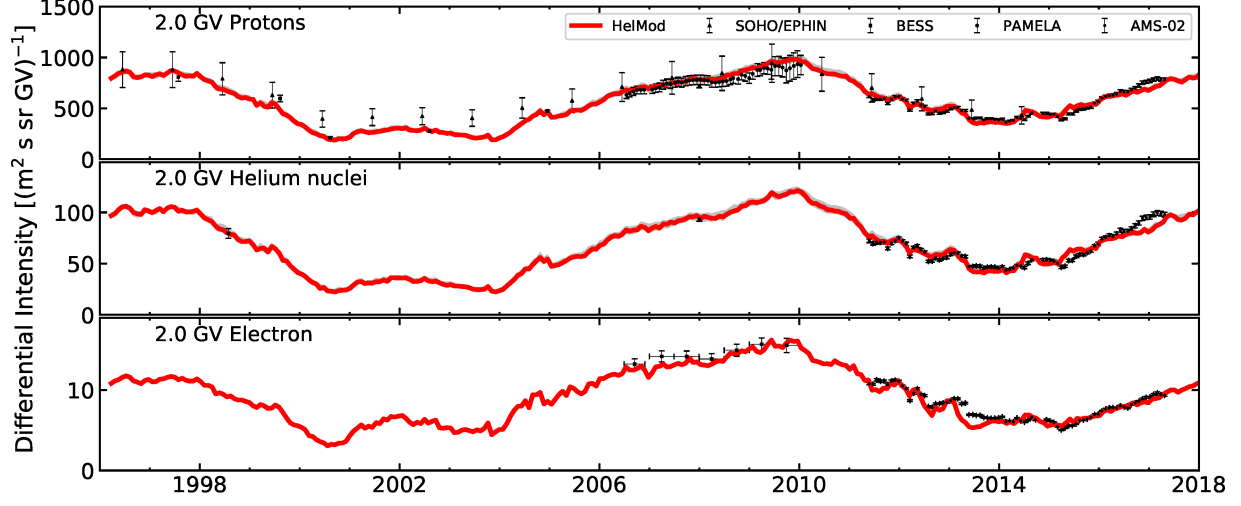
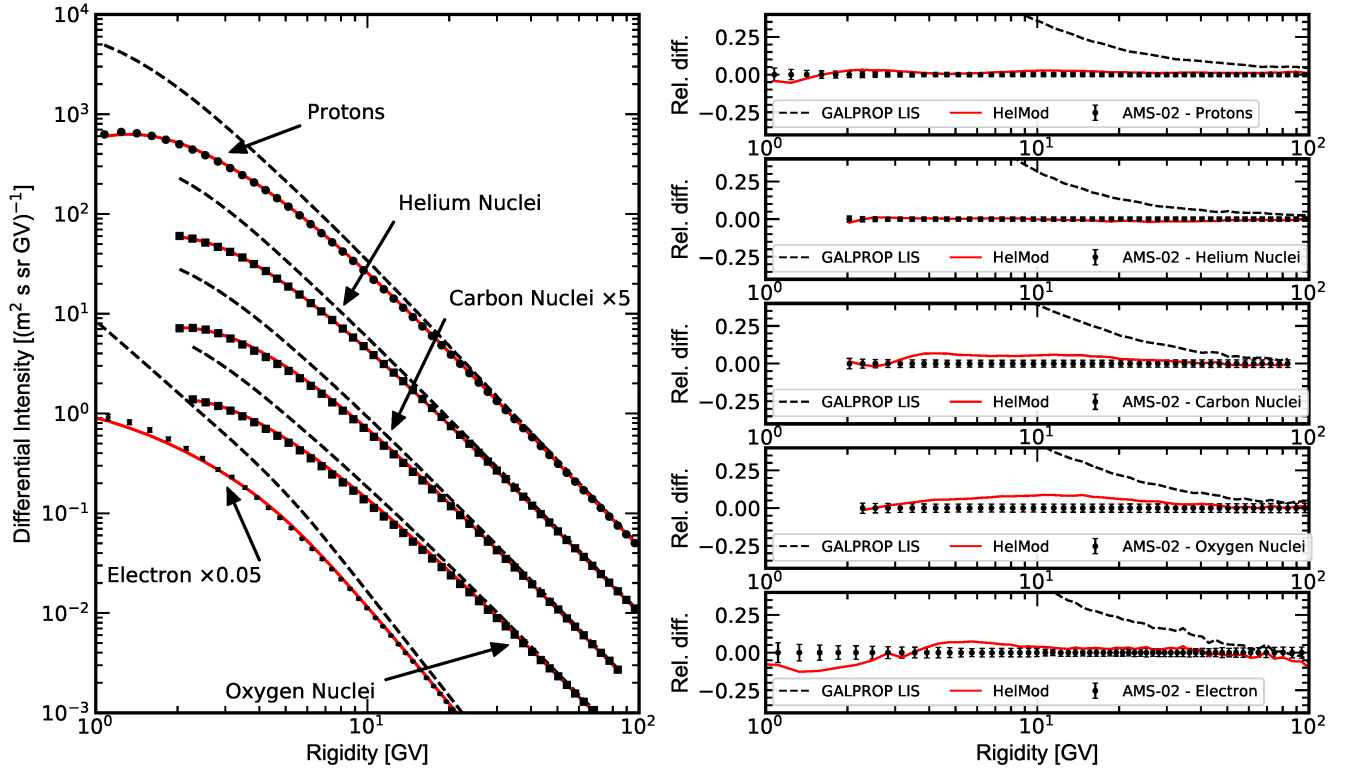


Figure 8: Modulated spectra observed by AMS-02 (points), for protons ([Aguilar et al., 2015b](#)), electrons ([Aguilar et al., 2014b](#)) and nuclei, i.e., helium, carbon and oxygen ([Aguilar et al., 2017](#)), compared with HELMOD-GALPROP LISs (dashed lines, already shown in Fig. 1) from [Boschini et al. \(2017\)](#), [Boschini et al. \(2018b\)](#), and [Boschini et al. \(2018c\)](#) along with HELMOD version 4 modulated spectra (red solid line). On the left panel, differential intensities are reported. On the right panel, the relative difference of experimental data with HELMOD version 4 simulations and LISs are shown.



the corresponding R'_{TS} can be obtained using SW speed measurements from Voyager 2, Wind, ACE, Ulysses (also NASA-OMNIweb). In fact, for any position on TS calculated from Eq. (7), one can determine that particular value R'_{TS} at which the SW has a speed u'_{2TS} such that it reaches the HP position at the exact crossing date of Voyager 1. The average of the so obtained R'_{TS} values is 77.2 ± 2.6 AU. Thus, one finds that numerically Eq. (17) can be re-written as

$$\frac{R_{HP}}{R'_{TS}} = \sqrt[4]{T_H} = 1.58 \pm 0.05.$$

In Fig. 4 (Fig. 5) the time variation of the average positions of the HP (solid line) from 1977 to up to the end of 2018 is shown at 34.5° (-32.2°). By inspecting the two figures, one can remark that the predicted value of 120.7 AU at the time of the Voyager 2 HP crossing²⁴ (5 November 2018) is in agreement with that observed, i.e., 119 AU (NASA's Voyager team, 2018).

5. Solar Modulation in the outer heliosphere

As discussed in Kóta (2016), the diffusion and drift motion of CRs in the HS should depend on the structure of the HMF beyond the TS. Inside the HS, although several authors propose more complex models (see, e.g., Zhang et al., 2015; Kóta, 2016), to a first approximation, currently in HELMOD we implemented a spherical symmetric propagation description depending on a scalar diffusion coefficient $k_{hs} = 2.5 \times 10^{-5} \cdot \beta \cdot P \text{ AU}^2 \text{ s}^{-1}$. Scherer et al. (2011) already discussed that in the HS the plasma flow is to a good approximation incompressible (see also discussion in Sect. 4) and, therefore, divergence-free, implying vanishing adiabatic energy changes. Under such a condition Parker equation reduced to (e.g. see Scherer et al. 2011; Bobik et al. 2016):

$$\frac{\partial U}{\partial t} = \frac{1}{R^2} \frac{\partial}{\partial R} \left(R^2 k_{hs} \frac{\partial}{\partial R} U \right) - \frac{1}{R^2} \frac{\partial R^2 V_{sw,2R} U}{\partial R}. \quad (19)$$

where $V_{sw,2R}$ is the radial SW speed in the HS (see Eq. (6)). The diffusion coefficient was tuned in order to reproduce Voyager proton spectra during the journey in the HS (see discussion on Fig. 6 in Sect. 6.2).

In order to account for the strong modulation effect observed by Voyager 1 in 2012 before the HP crossing (see, e.g., Zhang et al., 2015, and references therein), the diffusion coefficient must be reduced by a factor 50 in the outermost layer, 1–2 AU thick, thus allowing the creation of a diffusion barrier against low energy CRs propagation. As shown in Fig. 6 (discussed in Sect. 6.2), available data of CR in HS, from Voyagers probes, are well reproduced within this simplified scenario.

6. Solar Modulation in the inner part of the heliosphere

Modeling solar modulation for a time period covering more than one solar cycle represents a challenge due to the large variability of the interplanetary environment not only from the solar minimum up to the solar maximum but also from one cycle to the next one. Nevertheless, particle modulation occurring during solar minima is well described by the transport model – including magnetic drift – presented in Sect. 2. Other approaches leading to similar results can be found, e.g., in Potgieter et al. (2013) and reference there in (see also, Ferreira and Potgieter, 2004; Corti et al., 2019). HELMOD code (Gervasi et al., 1999; Bobik et al., 2012, 2013; Boschini et al., 2018a) is a Monte Carlo numerical code that solves Eq. (1) using Stochastic Differential Equations, in a backward-in-time approach described, e.g., in Bobik et al. (2016).

The current version of HELMOD model treats solar modulation separately in the inner and in the outer heliosphere. In the inner heliosphere, confined by the slightly asymmetric TS described in Sect. 3, we use the time-dependent propagation model described in appendix A.1 of Boschini et al. (2018a). The current model exhibits a weak longitudinal dependence that originates from the presence of the asymmetric TS. Nevertheless, at 1AU the difference of computed flux between nose and tail directions of the heliosphere is less than the numerical method uncertainties ($< a \text{ few } \%$).

HELMOD was tuned on proton flux in both low and high solar activity periods, allowing to reproduce intensity variation along the complete cycle duration. The qualitative agreement among experimental data and simulated spectra can be appreciated in Fig. 7, where HELMOD results are compared to protons, helium nuclei and electrons differential intensities at 2 GV from the begin of 1996 up to the end of 2017. For such a comparison we include data from AMS-02 (Aguilar et al., 2018a,d), PAMELA (Adriani et al., 2013, 2015), BESS (Shikaze et al., 2007) and SOHO/EPHIN (Kühl et al., 2016), thus covering the last two solar cycles. In Fig. 8 representative examples of comparison of HELMOD 4 simulated spectra with AMS-02 data (Aguilar et al., 2015a,b, 2014b; Aguilar et al., 2017) are presented²⁵; the agreement, as shown in right panels of Fig. 8, is better than previously obtained and showed in Figure 11 of (Boschini et al., 2017), in Figure 3 of (Boschini et al., 2018c), in Figure 4 and 5 of (Boschini et al., 2018b), and, finally, reported above in Fig. 1.

6.1. Transition from low to high solar activity

The high accuracy of newest AMS-02 data, that presented differential intensity of protons, helium nuclei and electron from 2011 to 2017 down to 1 GV (Aguilar et al.,

²⁴ Due to the slow speed of the spacecraft, we cannot exclude a further crossing of HP boundary in the future.

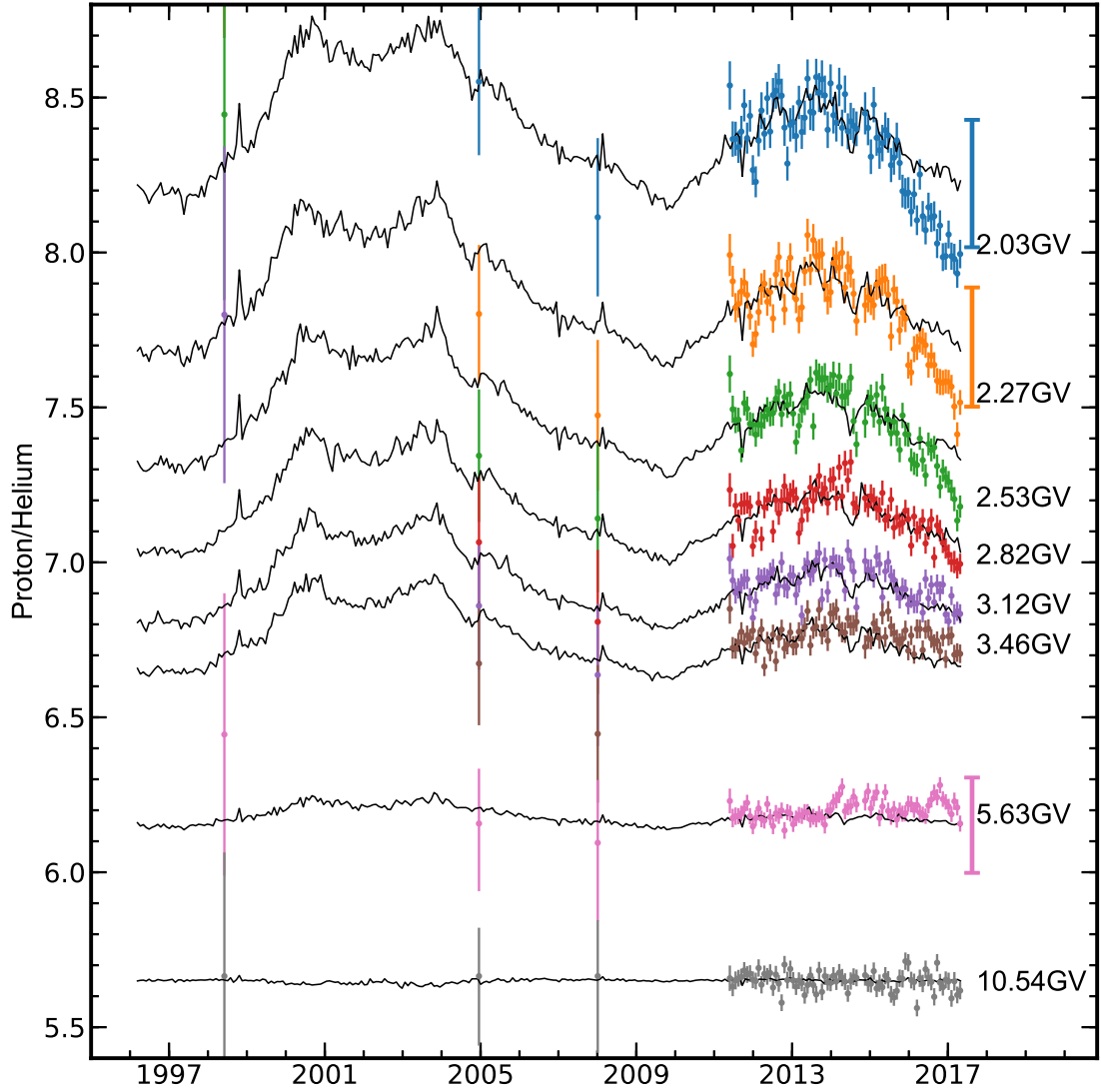
²⁵ Calculation for different experimental data-sets can be downloaded using the HelMod Web Modulator (www.helmod.org)

Table 2: HELMOD parameters for the transition function described in Eq. (21).

				Ascending		Descending	
		F_{\min}	F_{\max}	α_0	s	α_0	s
$P_{0,d}$		0.5	4	73	1	63	10
$P_{0,NS}$		0.5	SSN*/50	73	1	63	10
K_c	$q > 0; A > 0$	3	1	40	18	53	5
	$q > 0; A < 0$	1	1	-	-	-	-
	$q < 0; A < 0$	3	1	40	18	53	5
	$q < 0; A > 0$	0.7	1	47	5.8	58.4	5.8
g_{low}	$e^+; e^-$	0.4	0	67	20	45	10
	p; Ions	0.5	0	60	9	45	10
R_c		4	1	60	9	45	10

* SSN is the smoothed sunspot number from SIDC ([World Data Center SILSO, 1964-2015](#); [Clette et al., 2015](#)).

Figure 9: The p/He flux ratio as function of time for 9 characteristic rigidity bins as reported in [Aguilar et al. \(2018a\)](#). HELMOD version 4 simulation (solid line) – obtained using the corresponding LISs from [Boschini et al. \(2017\)](#), [Boschini et al. \(2018b\)](#) – is compared with AMS-02 and BESS observation at nearest rigidity bin. Vertical bars on the right side represent 5% variation.



2018a,d), made possible to study with great details the solar maximum of cycle 24. It is well known that the effects related to particle drift processes are reduced at solar maximum due to the more chaotic structure of the HMF (see, e.g., Minnie et al., 2007; Burger and Visser, 2010). This is usually accounted in Eq. (1) by means of a partial (or, eventually, complete) suppression of the drift term during the solar maxima (see, e.g., discussion in Ferreira and Potgieter, 2004). Moreover, the presence of turbulences in the interplanetary medium should reduce the global effect of CR drift at very low energy also during solar minimum periods. In literature this effect is usually taken into account by a *drift suppression factor*, f_s , that is more relevant at rigidities below 1 GV (see, e.g., Equation 2 in Engelbrecht et al., 2017, and references therein):

$$f_s = \frac{(P/P_{0,d})^2}{1 + (P/P_{0,d})^2}. \quad (20)$$

$P_{0,d}$, in GV, is an ad-hoc parameter tuned to achieve the agreement with data. In the present model this *suppression factor* is applied with a different magnitude both on *regular drift* and *neutral sheet drift*. The parameters $P_{0,d}$ (for *regular drift* suppression) and $P_{0,NS}$ (for *neutral sheet drift* suppression) were derived by comparison with time dependent spectra measured by AMS-02. A crosscheck of such a parametrization was done using BESS data during solar maximum of solar cycle 23. Some of these parameters – i.e. $P_{0,d}$, $P_{0,NS}$, K_c , g_{low} and R_c – change their value with solar activity by means of a transition function from solar minimum to maximum assuming the form:

$$F(\alpha_t) = \frac{F_{\min} + F_{\max}}{2} - \frac{F_{\min} - F_{\max}}{2} \tanh \left[\frac{\alpha_t - \alpha_0}{s} \right]. \quad (21)$$

Parameters of Eq. (21) are reported in Table 2; F_{\min} represents the parameter value at solar minimum, F_{\max} at solar maximum, α_t is the "L"-model tilt angle of neutral sheet as computed by Wilcox Observatory (Hoeksema, 1995; WSO, 2018, see discussion in Bobik et al. 2012, 2013; Boschini et al. 2018a), α_0 and s are parameters defining the time and the sharpness of the transition.

By inspection of Table 2, it is worth to note that the *neutral sheet drift suppression* at solar maximum depends on the amount of solar disturbances (parametrized by smoothed sunspot number as a proxy): the higher the solar activity, the broader the rigidity range of drift suppression. Conversely, in the case of *regular drift suppression* factor the rigidity range at maximum is always the same.

By tuning AMS-02 and PAMELA measurements, i.e., at solar maximum and at solar minimum respectively, we found different values of g_{low} and R_c parameters to be employed in Eq. (2). The transition between the two regimes was parametrized by means of Eq. (21). Parameters reported in Table 2 were crosschecked using BESS and AMS-01 data during the solar minimum between solar cycles 22 and 23. Finally the parallel component of the diffusion tensor is multiplied by a correction factor (K_c) that

rescales the absolute value of $K_{||}$ due to drift contribution (Boschini et al., 2018a). Such a correction is more important during solar minima when drift processes are relevant. The time evolution of K_c is still parametrized by means of Eq. (21) using the parameters reported in Table 2.

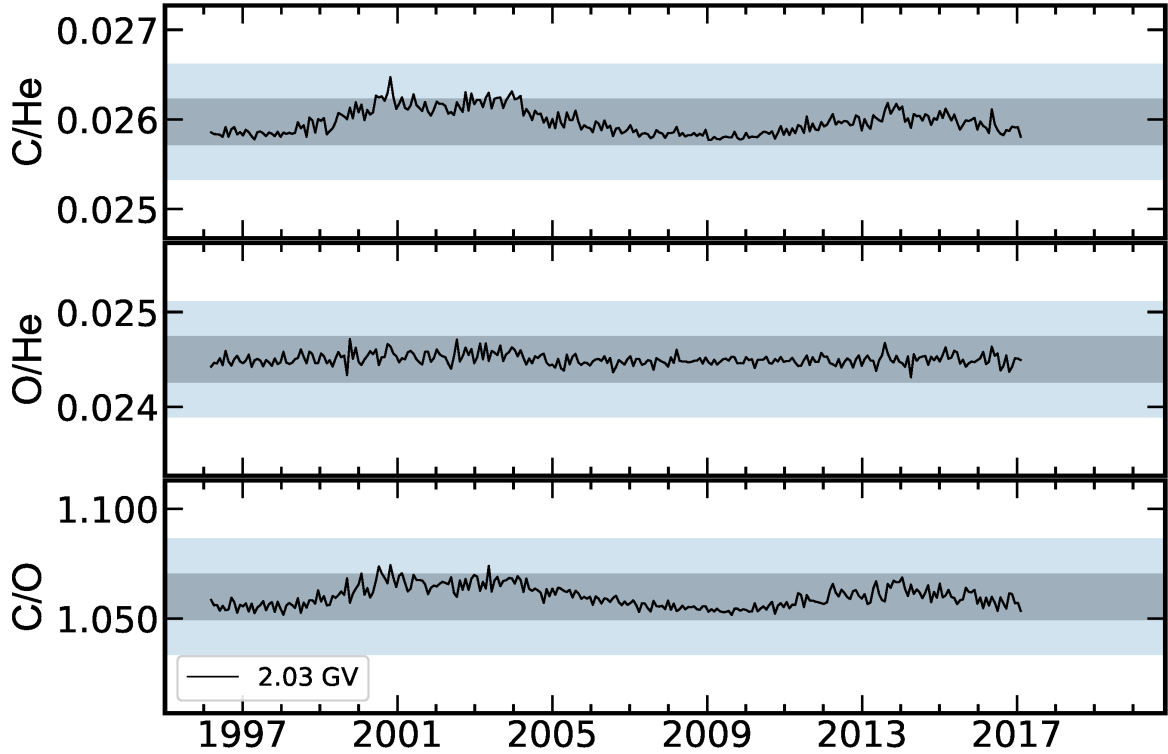
6.2. Discussion

After being tuned using proton flux, HELMOD model is then applied to evaluate nuclei and electron spectra along the last two solar cycles. In Fig. 7 the HELMOD simulations for 2 GV protons, helium nuclei and electrons are shown. Typical rms discrepancy between data and simulations is of the order of 7%. This value becomes 10% if SOHO data are included. Discrepancies greater than these values are related to specific limited periods that need further investigations. As indicated in right panel of Fig. 8, at 20 GV modulation is still active. For example, the difference between LISs and AMS-02 observed spectra is 15.7%, 13.2% and 21.8% for protons, helium nuclei and electrons respectively (see also Figure 11 of Boschini et al. 2017 and Figure 3 of Boschini et al. 2018c). This difference is slightly dependent on time, it is almost charge independent, and it is mostly related to diffusion term of Eq. (1).

HELMOD can be also used to estimate the GCR omnidirectional intensities at large distances from Earth and outside the ecliptic plane in comparison with data from Voyager (see, e.g., McDonald and Lal, 1986; Cummings et al., 1987; Venkatesan and Badruddin, 1990; Zeldovich et al., 2005) and Ulysses (see Heber 2011 or Heber and Potgieter 2006 for recent reviews) probes. HELMOD already demonstrated, also with previous versions, its capability to reproduce qualitatively and quantitatively the latitudinal profile of the GCR intensity as observed in the inner part of heliosphere by the Ulysses spacecraft. HELMOD 4.0 simulations confirm results obtained previously (e.g. see Bobik et al., 2013; Boschini et al., 2018a, 2017, 2018c). To account the radial dependence observed by Voyager probes, a systematic investigation of the parallel and perpendicular diffusion coefficients (Sect. 2) at large heliocentric distances was carried out. Several radial profiles for $K_{||}$ and K_{\perp} were tested (see, for example, Burger and Hattingh, 1998b; Laitinen et al., 2016; Moloto et al., 2018). The best agreement was obtained using the analytical expression in Eq. (2), implying a larger diffusion coefficient – and, in turn, less modulation effect – in the inner part of heliosphere with respect to a simpler radial dependence. In Fig. 6 HELMOD results are compared with the experimental data from Voyager 1 and Voyager 2 at 0.25 GeV (NASA-Voyager, 2018). Current model shows a general good agreement with experimental data except for some specific period, i.e. declining phase in 1987, that needs further investigation.

Recent measurements of AMS-02 (Aguilar et al., 2018a) pointed out that the p/He ratio has a long-term dependence on time for rigidities lower than ~ 3 GV. In Fig. 9

Figure 10: Nuclei flux ratios from 1996 to 2017 for ~ 2 GV determined by means of HELMOD version 4 simulations, using the corresponding LISs from Boschini et al. (2018b), are reported with solid line. Top panel shows carbon over helium ratio, mid panel oxygen over helium ratio and low panel carbon over oxygen ratio. Dark (light) blue regions represent the 2% (5%) variation.



we reported the p/He ratios obtained from HelMod model from 1996 to 2017 compared with observations made by AMS-02 and BESS (Alcaraz et al., 2000b; Aguilar et al., 2002; Abe et al., 2016; Aguilar et al., 2018a). By inspection of HelMod results, one can note that the p/He ratio exhibits a time dependence with a periodicity longer than the duration of the AMS-02 data taking. For the first time, the high precision data from AMS-02 allowed to highlight the variation of p/He ratio over a long period of time. In Fig. 10 the HELMOD predictions are shown to illustrate the time dependence of the flux ratios for carbon over helium, oxygen over helium and carbon over oxygen at ~ 2 GV from 1996 to 2017; in Fig. 10 the HelMod predictions are shown to illustrate the time dependence of the flux ratios for carbon over helium, oxygen over helium and carbon over oxygen at 2 GV from 1996 to 2017; these ratios are predicted to be almost independent of time also at such a low rigidity. These simulations indicate that a tiny variation with time – slightly lower than those presented in Fig. 9 for the p/He ratio – is exhibited with differences on average of the order of 2% (dark blue bands) among solar maxima and solar minima.

7. Conclusions

In this work, we presented the current version 4 of HELMOD model which deals with the modulation pro-

cesses affecting GCRs, during their propagation in the inner and outer regions of the heliosphere.

In the present code particular attention was paid to deal with high solar activity periods, by comparing our simulations with observations made by AMS-02, and on transitions from/to low solar minima. This was achieved by introducing a *drift suppression factor* and particle diffusion parameters which depend on the level of solar disturbances. In HELMOD, time-dependent heliospheric parameters were tuned by comparison with the statistically dominant proton spectra, then used to derive the modulated spectra for all GCR species. The solidity of HELMOD model was demonstrated by its capability of reproducing protons, nuclei and electrons CRs spectra observed during solar cycles 23-24 by several detectors, for instance, PAMELA, BESS and AMS-02.

In the present model the actual dimensions of the heliosphere and its boundaries were taken into account based on Voyager probes observations. The modulation in HS was investigated by means of a 1-D solution, which turns out to be well reproducing the Voyager measurements, for instance, those regarding the intensity of GCRs as function of heliocentric distance for the Voyager 1 (Voyager 2) energy channel of 0.25 GeV/nuc (0.26 GeV/nuc). In addition, the agreement is also found among the HELMOD simulations and Voyager intensity measurements in the inner part of the heliosphere. This is an indication of the ap-

appropriateness of the modulation mechanisms implemented in the model.

Acknowledgements

This work is supported by ASI (Agenzia Spaziale Italiana) under contract ASI-INFN I/002/13/0 and ESA (European Space Agency) contract 4000116146/16/NL/HK.

We acknowledge the NMDB database (www.nmdb.eu), supported under the European Union's FP7 programme (contract no. 213007) for providing data. The data from McMurdo were provided by the University of Delaware with support from the U.S. National Science Foundation under grant ANT-0739620. Finally, we acknowledge the use of NASA/GSFC's Space Physics Data Facility's OMNIWeb service, and OMNI data.

We wish to specially thank Pavol Bobik, Giuliano Boella, Davide Grandi, Karel Kudela, Simonetta Pensotti, Marian Putis, Davide Rozza, Mauro Tacconi and Mario Zannoni for their support to HELMOD code and suggestions.

References

References

- Abdo, A.A., Ackermann, M., Ajello, M., et al., 2009. Measurement of the Cosmic Ray $e^+ + e^-$ Spectrum from 20 GeV to 1 TeV with the Fermi Large Area Telescope. *Physical Review Letters* 102, 181101. doi:[10.1103/PhysRevLett.102.181101](https://doi.org/10.1103/PhysRevLett.102.181101), [arXiv:0905.0025](https://arxiv.org/abs/0905.0025).
- Abe, K., Fuke, H., Haino, S., et al., 2008. Measurement of the cosmic-ray low-energy antiproton spectrum with the first BESS-Polar Antarctic flight. *Physics Letters B* 670, 103–108. doi:[10.1016/j.physletb.2008.10.053](https://doi.org/10.1016/j.physletb.2008.10.053).
- Abe, K., Fuke, H., Haino, S., et al., 2016. Measurements of Cosmic-Ray Proton and Helium Spectra from the BESS-Polar Long-duration Balloon Flights over Antarctica. *Astrophys. J.* 822, 65. doi:[10.3847/0004-637X/822/2/65](https://doi.org/10.3847/0004-637X/822/2/65), [arXiv:1506.01267](https://arxiv.org/abs/1506.01267).
- Adriani, O., Barbarino, G.C., Bazilevskaya, G.A., et al., 2009a. An anomalous positron abundance in cosmic rays with energies 1.5–100 GeV. *Nature* 458, 607–609. doi:[10.1038/nature07942](https://doi.org/10.1038/nature07942), [arXiv:0810.4995](https://arxiv.org/abs/0810.4995).
- Adriani, O., Barbarino, G.C., Bazilevskaya, G.A., et al., 2009b. New Measurement of the Antiproton-to-Proton Flux Ratio up to 100 GeV in the Cosmic Radiation. *Physical Review Letters* 102, 051101. doi:[10.1103/PhysRevLett.102.051101](https://doi.org/10.1103/PhysRevLett.102.051101), [arXiv:0810.4994](https://arxiv.org/abs/0810.4994).
- Adriani, O., Barbarino, G.C., Bazilevskaya, G.A., et al., 2010. PAMELA Results on the Cosmic-Ray Antiproton Flux from 60 MeV to 180 GeV in Kinetic Energy. *Physical Review Letters* 105, 121101. doi:[10.1103/PhysRevLett.105.121101](https://doi.org/10.1103/PhysRevLett.105.121101), [arXiv:1007.0821](https://arxiv.org/abs/1007.0821).
- Adriani, O., Barbarino, G.C., Bazilevskaya, G.A., et al., 2011. PAMELA Measurements of Cosmic-Ray Proton and Helium Spectra. *Science* 332, 69. doi:[10.1126/science.1199172](https://doi.org/10.1126/science.1199172), [arXiv:1103.4055](https://arxiv.org/abs/1103.4055).
- Adriani, O., Barbarino, G.C., Bazilevskaya, G.A., et al., 2013. Time dependence of the proton flux measured by pameela during the 2006 july-2009 december solar minimum. *Astrophys. J.* 765, 91. doi:[10.1088/0004-637X/765/2/91](https://doi.org/10.1088/0004-637X/765/2/91), [arXiv:1301.4108](https://arxiv.org/abs/1301.4108).
- Adriani, O., Barbarino, G.C., Bazilevskaya, G.A., et al., 2015. Time Dependence of the e^- Flux Measured by PAMELA during the July 2006–December 2009 Solar Minimum. *Astrophys. J.* 810, 142. doi:[10.1088/0004-637X/810/2/142](https://doi.org/10.1088/0004-637X/810/2/142), [arXiv:1512.01079](https://arxiv.org/abs/1512.01079).
- Aguilar, M., Aisa, D., Alpat, B., et al. (AMS Collaboration), 2014a. Precision measurement of the $(e^+ + e^-)$ flux in primary cosmic rays from 0.5 gev to 1 tev with the alpha magnetic spectrometer on the international space station. *Phys. Rev. Lett.* 113, 221102. URL: <http://link.aps.org/doi/10.1103/PhysRevLett.113.221102>, doi:[10.1103/PhysRevLett.113.221102](https://doi.org/10.1103/PhysRevLett.113.221102).
- Aguilar, M., Aisa, D., Alpat, B., et al. (AMS Collaboration), 2015a. Precision measurement of the helium flux in primary cosmic rays of rigidities 1.9 gv to 3 tv with the alpha magnetic spectrometer on the international space station. *Phys. Rev. Lett.* 115, 211101. URL: <http://link.aps.org/doi/10.1103/PhysRevLett.115.211101>, doi:[10.1103/PhysRevLett.115.211101](https://doi.org/10.1103/PhysRevLett.115.211101).
- Aguilar, M., Aisa, D., Alpat, B., et al. (AMS Collaboration), 2015b. Precision measurement of the proton flux in primary cosmic rays from rigidity 1 gv to 1.8 tv with the alpha magnetic spectrometer on the international space station. *Phys. Rev. Lett.* 114, 171103. URL: <http://link.aps.org/doi/10.1103/PhysRevLett.114.171103>, doi:[10.1103/PhysRevLett.114.171103](https://doi.org/10.1103/PhysRevLett.114.171103).
- Aguilar, M., Aisa, D., Alvino, A., et al. ((AMS Collaboration)), 2014b. Electron and positron fluxes in primary cosmic rays measured with the alpha magnetic spectrometer on the international space station. *Phys. Rev. Lett.* 113, 121102. URL: <http://link.aps.org/doi/10.1103/PhysRevLett.113.121102>, doi:[10.1103/PhysRevLett.113.121102](https://doi.org/10.1103/PhysRevLett.113.121102).
- Aguilar, M., Alcaraz, J., Allaby, J., et al., 2002. The Alpha Magnetic Spectrometer (AMS) on the International Space Station: Part I - results from the test flight on the space shuttle. *Phys. Rep.* 366, 331–405. doi:[10.1016/S0370-1573\(02\)00013-3](https://doi.org/10.1016/S0370-1573(02)00013-3).
- Aguilar, M., Alcaraz, J., Allaby, J., et al., 2007. Cosmic-ray positron fraction measurement from 1 to 30 GeV with AMS-01. *Physics Letters B* 646, 145–154. doi:[10.1016/j.physletb.2007.01.024](https://doi.org/10.1016/j.physletb.2007.01.024), [arXiv:astro-ph/0703154](https://arxiv.org/abs/astro-ph/0703154).
- Aguilar, M., Ali Cavasonza, L., Alpat, B., Ambrosi, G., Arruda, L., Attig, N., Aupetit, S., Azzarello, P., Bachlechner, A., Barao, F., et al., 2017. Observation of the Identical Rigidity Dependence of He, C, and O Cosmic Rays at High Rigidities by the Alpha Magnetic Spectrometer on the International Space Station. *Physical Review Letters* 119, 251101. doi:[10.1103/PhysRevLett.119.251101](https://doi.org/10.1103/PhysRevLett.119.251101).
- Aguilar, M., Ali Cavasonza, L., Alpat, B., Ambrosi, G., Arruda, L., Attig, N., Aupetit, S., Azzarello, P., Bachlechner, A., Barao, F., et al. (AMS Collaboration), 2018a. Observation of fine time structures in the cosmic proton and helium fluxes with the alpha magnetic spectrometer on the international space station. *Phys. Rev. Lett.* 121, 051101. URL: <https://link.aps.org/doi/10.1103/PhysRevLett.121.051101>, doi:[10.1103/PhysRevLett.121.051101](https://doi.org/10.1103/PhysRevLett.121.051101).
- Aguilar, M., Ali Cavasonza, L., Alpat, B., Ambrosi, G., Arruda, L., Attig, N., Aupetit, S., Azzarello, P., Bachlechner, A., Barao, F., et al., 2018b. Precision Measurement of Cosmic-Ray Nitrogen and its Primary and Secondary Components with the Alpha Magnetic Spectrometer on the International Space Station. *Physical Review Letters* 121, 051103. doi:[10.1103/PhysRevLett.121.051103](https://doi.org/10.1103/PhysRevLett.121.051103).
- Aguilar, M., Ali Cavasonza, L., Alpat, B., et al. (AMS Collaboration), 2016. Antiproton flux, antiproton-to-proton flux ratio, and properties of elementary particle fluxes in primary cosmic rays measured with the alpha magnetic spectrometer on the international space station. *Phys. Rev. Lett.* 117, 091103. URL: <http://link.aps.org/doi/10.1103/PhysRevLett.117.091103>, doi:[10.1103/PhysRevLett.117.091103](https://doi.org/10.1103/PhysRevLett.117.091103).
- Aguilar, M., Ali Cavasonza, L., Ambrosi, G., Arruda, L., Attig, N., Aupetit, S., Azzarello, P., Bachlechner, A., Barao, F., Barrau, A., et al., 2016. Precision Measurement of the Boron to Carbon Flux Ratio in Cosmic Rays from 1.9 GV to 2.6 TV with the Alpha Magnetic Spectrometer on the International Space Station. *Physical Review Letters* 117, 231102. doi:[10.1103/PhysRevLett.117.231102](https://doi.org/10.1103/PhysRevLett.117.231102).
- Aguilar, M., Ali Cavasonza, L., Ambrosi, G., Arruda, L., Attig, N., Aupetit, S., Azzarello, P., Bachlechner, A., Barao, F., Barrau, A., et al., 2018c. Observation of New Properties of Secondary Cosmic Rays Lithium, Beryllium, and Boron by the Alpha Magnetic Spectrometer on the International Space Station. *Physical Review*

- Letters 120, 021101. doi:[10.1103/PhysRevLett.120.021101](https://doi.org/10.1103/PhysRevLett.120.021101).
- Aguilar, M., Cavasonza, L.A., Ambrosi, G., Arruda, L., Atig, N., Aupetit, S., Azzarello, P., Bachlechner, A., Barao, F., Barrau, A., et al., 2018d. Observation of Complex Time Structures in the Cosmic-Ray Electron and Positron Fluxes with the Alpha Magnetic Spectrometer on the International Space Station. *Physical Review Letters* 121, 051102. doi:[10.1103/PhysRevLett.121.051102](https://doi.org/10.1103/PhysRevLett.121.051102).
- Alcaraz, J., Alpat, B., Ambrosi, G., et al., 2000a. Cosmic protons. *Physics Letters B* 490, 27–35. doi:[10.1016/S0370-2693\(00\)00970-9](https://doi.org/10.1016/S0370-2693(00)00970-9).
- Alcaraz, J., Alpat, B., Ambrosi, G., et al., 2000b. Helium in near Earth orbit. *Physics Letters B* 494, 193–202. doi:[10.1016/S0370-2693\(00\)01193-X](https://doi.org/10.1016/S0370-2693(00)01193-X).
- Alcaraz, J., Alpat, B., Ambrosi, G., et al., 2000c. Leptons in near earth orbit. *Physics Letters B* 484, 10–22. doi:[10.1016/S0370-2693\(00\)00588-8](https://doi.org/10.1016/S0370-2693(00)00588-8).
- Alcaraz, J., Alvisi, D., Alpat, B., et al., 2000d. Protons in near earth orbit. *Physics Letters B* 472, 215–226. doi:[10.1016/S0370-2693\(99\)01427-6](https://doi.org/10.1016/S0370-2693(99)01427-6), [arXiv:hep-ex/0002049](https://arxiv.org/abs/hep-ex/0002049).
- Axford, W.I., 1972. The Interaction of the Solar Wind With the Interstellar Medium. *NASA Special Publication* 308, 609.
- Bieber, J.W., Matthaeus, W.H., Smith, C.W., et al., 1994. Proton and electron mean free paths: The Palmer consensus revisited. *Astrophys. J.* 420, 294–306. doi:[10.1086/173559](https://doi.org/10.1086/173559).
- Bobik, P., Boella, G., Boschini, M.J., et al., 2012. Systematic Investigation of Solar Modulation of Galactic Protons for Solar Cycle 23 Using a Monte Carlo Approach with Particle Drift Effects and Latitudinal Dependence. *Astrophys. J.* 745, 132. doi:[10.1088/0004-637X/745/2/132](https://doi.org/10.1088/0004-637X/745/2/132), [arXiv:1110.4315](https://arxiv.org/abs/1110.4315).
- Bobik, P., Boella, G., Boschini, M.J., et al., 2013. Latitudinal dependence of cosmic rays modulation at 1 au and interplanetary magnetic field polar correction. *Advances in Astronomy* 2013. doi:[10.1155/2013/793072](https://doi.org/10.1155/2013/793072), [arXiv:1212.1559](https://arxiv.org/abs/1212.1559).
- Bobik, P., Boschini, M.J., Della Torre, S., et al., 2016. On the forward-backward-in-time approach for monte carlo solution of parker's transport equation: One-dimensional case. *Journal of Geophysical Research: Space Physics* 121, 3920–3930. URL: <http://dx.doi.org/10.1002/2015JA022237>, doi:[10.1002/2015JA022237](https://doi.org/10.1002/2015JA022237). 2015JA022237.
- Boella, G., Gervasi, M., Potenza, M.A.C., et al., 1998. Modulated antiproton fluxes for interstellar production models. *Astroparticle Physics* 9, 261–267. doi:[10.1016/S0927-6505\(98\)00022-X](https://doi.org/10.1016/S0927-6505(98)00022-X).
- Boezio, M., Carlson, P., Francke, T., et al., 1999. The Cosmic-Ray Proton and Helium Spectra between 0.4 and 200 GV. *Astrophys. J.* 518, 457–472. doi:[10.1086/307251](https://doi.org/10.1086/307251).
- Boschini, M., Della Torre, S., Gervasi, M., La Vacca, G., Rancoita, P., 2018a. Propagation of cosmic rays in heliosphere: the helmod model. *Adv. Space Res.* 62, 2859 – 2879. URL: <https://arxiv.org/abs/1704.03733>, doi:[10.1016/j.asr.2017.04.017](https://doi.org/10.1016/j.asr.2017.04.017). origins of Cosmic Rays.
- Boschini, M.J., Della Torre, S., Gervasi, M., Grandi, D., Jóhannesson, G., Kachelriess, M., La Vacca, G., Masi, N., Moskalenko, I.V., Orlando, E., Ostapchenko, S.S., Pensotti, S., Porter, T.A., Quadrani, L., Rancoita, P.G., Rozza, D., Tacconi, M., 2017. Solution of Heliospheric Propagation: Unveiling the Local Interstellar Spectra of Cosmic-ray Species. *Astrophys. J.* 840, 115. doi:[10.3847/1538-4357/aa6e4f](https://doi.org/10.3847/1538-4357/aa6e4f), [arXiv:1704.06337](https://arxiv.org/abs/1704.06337).
- Boschini, M.J., Della Torre, S., Gervasi, M., Grandi, D., Jóhannesson, G., La Vacca, G., Masi, N., Moskalenko, I.V., Pensotti, S., Porter, T.A., Quadrani, L., Rancoita, P.G., Rozza, D., Tacconi, M., 2018b. Deciphering the local interstellar spectra of primary cosmic-ray species with helmod. *The Astrophysical Journal* 858, 61. URL: <https://arxiv.org/abs/1804.06956>, doi:[10.3847/1538-4357/aabc54](https://doi.org/10.3847/1538-4357/aabc54).
- Boschini, M.J., Della Torre, S., Gervasi, M., Grandi, D., Jóhannesson, G., La Vacca, G., Masi, N., Moskalenko, I.V., Pensotti, S., Porter, T.A., Quadrani, L., Rancoita, P.G., Rozza, D., Tacconi, M., 2018c. Helmod in the works: From direct observations to the local interstellar spectrum of cosmic-ray electrons. *Astrophys. J.* 854, 94. URL: <https://arxiv.org/abs/1704.06337>, doi:[10.3847/1538-4357/aaa75e](https://doi.org/10.3847/1538-4357/aaa75e).
- Bottino, A., Donato, F., Fornengo, N., et al., 1998. Which fraction of the measured cosmic-ray antiprotons might be due to neutralino annihilation in the galactic halo? *Phys. Rev. D.* 58, 123503. doi:[10.1103/PhysRevD.58.123503](https://doi.org/10.1103/PhysRevD.58.123503), [arXiv:astro-ph/9804137](https://arxiv.org/abs/astro-ph/9804137).
- Burger, R.A., Hattingh, M., 1998a. Toward a Realistic Diffusion Tensor for Galactic Cosmic Rays. *Astrophys. J.* 505, 244–251. doi:[10.1086/306152](https://doi.org/10.1086/306152).
- Burger, R.A., Hattingh, M., 1998b. Toward a Realistic Diffusion Tensor for Galactic Cosmic Rays. *Astrophys. J.* 505, 244–251. doi:[10.1086/306152](https://doi.org/10.1086/306152).
- Burger, R.A., Krüger, T.P.J., Hitge, M., et al., 2008. A Fisk-Parker Hybrid Heliospheric Magnetic Field With a Solar-Cycle Dependence. *Astrophys. J.* 674, 511–519. doi:[10.1086/525039](https://doi.org/10.1086/525039).
- Burger, R.A., Visser, D.J., 2010. Reduction of Drift Effects due to Solar Wind Turbulence. *Astrophys. J.* 725, 1366–1372. doi:[10.1088/0004-637X/725/1/1366](https://doi.org/10.1088/0004-637X/725/1/1366).
- Burlaga, L.F., 1984. MHD processes in the outer heliosphere. *Space Sci. Rev.* 39, 255–316. doi:[10.1007/BF00173902](https://doi.org/10.1007/BF00173902).
- Burlaga, L.F., Ness, N.F., 2016. Observations of the Interstellar Magnetic Field in the Outer Heliosheath: Voyager 1. *Astrophys. J.* 829, 134. doi:[10.3847/0004-637X/829/2/134](https://doi.org/10.3847/0004-637X/829/2/134).
- Burlaga, L.F., Ness, N.F., Acuña, M.H., Lepping, R.P., Connerney, J.E.P., Richardson, J.D., 2008. Magnetic fields at the solar wind termination shock. *Nature* 454, 75–77. doi:[10.1038/nature07029](https://doi.org/10.1038/nature07029).
- Bzowski, M., Swaczyna, P., Kubiak, M.A., Sokół, J.M., Fuselier, S.A., Galli, A., Heirtzler, D., Kucharek, H., Leonard, T.W., McComas, D.J., Möbius, E., Schwadron, N.A., Wurz, P., 2015. Interstellar Neutral Helium in the Heliosphere from IBEX Observations. III. Mach Number of the Flow, Velocity Vector, and Temperature from the First Six Years of Measurements. *Astrophys. J. Suppl. Series* 220, 28. doi:[10.1088/0067-0049/220/2/28](https://doi.org/10.1088/0067-0049/220/2/28), [arXiv:1510.04835](https://arxiv.org/abs/1510.04835).
- Cernuda, I., 2011. Anisotropies in the cosmic-ray electron spectrum: a way to discriminate between exotic and astrophysical sources? doi:[10.1142/9789814329033_0063](https://doi.org/10.1142/9789814329033_0063).
- Chang, J., Adams, J.H., Ahn, H.S., et al., 2008. An excess of cosmic ray electrons at energies of 300–800 GeV. *Nature* 456, 362–365. doi:[10.1038/nature07477](https://doi.org/10.1038/nature07477).
- Cirelli, M., Cline, J.M., 2010. Can multistate dark matter annihilation explain the high-energy cosmic ray lepton anomalies? *Phys. Rev. D.* 82, 023503. doi:[10.1103/PhysRevD.82.023503](https://doi.org/10.1103/PhysRevD.82.023503), [arXiv:1005.1779](https://arxiv.org/abs/1005.1779).
- Clette, F., Svalgaard, L., Cliver, E.W., et al., 2015. The new Sunspot and Group Numbers: a full recalibration. *IAU General Assembly* 22, 49591.
- Corti, C., Potgieter, M.S., Bindi, V., Consolandi, C., Light, C., Palermo, M., Popkow, A., 2019. Numerical Modeling of Galactic Cosmic-Ray Proton and Helium Observed by AMS-02 during the Solar Maximum of Solar Cycle 24. *Astrophys. J.* 871, 253. doi:[10.3847/1538-4357/aafac4](https://doi.org/10.3847/1538-4357/aafac4), [arXiv:1810.09640](https://arxiv.org/abs/1810.09640).
- Cummings, A.C., Stone, E.C., Heikkilä, B.C., Lal, N., Webber, W.R., Jóhannesson, G., Moskalenko, I.V., Orlando, E., Porter, T.A., 2016. Galactic Cosmic Rays in the Local Interstellar Medium: Voyager 1 Observations and Model Results. *Astrophys. J.* 831, 18. doi:[10.3847/0004-637X/831/1/18](https://doi.org/10.3847/0004-637X/831/1/18).
- Cummings, A.C., Stone, E.C., Webber, W.R., 1987. Latitudinal and radial gradients of anomalous and galactic cosmic rays in the outer heliosphere. *Geophysical Research Letters* 14, 174–177. doi:[10.1029/GL014i003p00174](https://doi.org/10.1029/GL014i003p00174).
- De Simone, N., Di Felice, V., Gieseler, J., et al., 2011. Latitudinal and radial gradients of galactic cosmic ray protons in the inner heliosphere - PAMELA and Ulysses observations. *Astrophysics and Space Sciences Transactions* 7, 425–434. doi:[10.5194/astra-7-425-2011](https://doi.org/10.5194/astra-7-425-2011).
- Decker, R.B., Krimigis, S.M., Roelof, E.C., Hill, M.E., Armstrong, T.P., Gloeckler, G., Hamilton, D.C., Lanzetta, L.J., 2005. Voyager 1 in the foreshock, termination shock, and heliosheath. *Science* 309, 2020–2024. URL: <http://science.sciencemag.org/content/309/5743/2020>, doi:[10.1126/science.1117569](https://doi.org/10.1126/science.1117569).

- Decker, R.B., Krimigis, S.M., Roelof, E.C., Hill, M.E., Armstrong, T.P., Gloeckler, G., Hamilton, D.C., Lanzerotti, L.J., 2008. Mediation of the solar wind termination shock by non-thermal ions. *Nature* 454, 67–70. doi:[10.1038/nature07030](https://doi.org/10.1038/nature07030).
- Della Torre, S., Gervasi, M., Rancoita, P.G., et al., 2015. Pulsar wind nebulae as a source of the observed electron and positron excess at high energy: The case of vela-x. *Journal of High Energy Astrophysics* 8, 27–34. doi:[10.1016/j.jheap.2015.08.001](https://doi.org/10.1016/j.jheap.2015.08.001), [arXiv:1508.01457](https://arxiv.org/abs/1508.01457).
- Dialynas, K., Krimigis, S.M., Mitchell, D.G., Decker, R.B., Roelof, E.C., 2017. The bubble-like shape of the heliosphere observed by Voyager and Cassini. *Nature Astronomy* 1, 0115. doi:[10.1038/s41550-017-0115](https://doi.org/10.1038/s41550-017-0115).
- Drake, J.F., Swisdak, M., Opher, M., 2015. A Model of the Heliosphere with Jets. *Astrophys. J. Letter* 808, L44. doi:[10.1088/2041-8205/808/2/L44](https://doi.org/10.1088/2041-8205/808/2/L44), [arXiv:1505.01451](https://arxiv.org/abs/1505.01451).
- Engelbrecht, N.E., Strauss, R.D., le Roux, J.A., Burger, R.A., 2017. Toward a Greater Understanding of the Reduction of Drift Coefficients in the Presence of Turbulence. *Astrophys. J.* 841, 107. doi:[10.3847/1538-4357/aa7058](https://doi.org/10.3847/1538-4357/aa7058).
- Evoli, C., Gaggero, D., Grasso, D., et al., 2008. Cosmic ray nuclei, antiprotons and gamma rays in the galaxy: a new diffusion model. *J. Cosmol. Astropart. P.* 10, 018. doi:[10.1088/1475-7516/2008/10/018](https://doi.org/10.1088/1475-7516/2008/10/018), [arXiv:0807.4730](https://arxiv.org/abs/0807.4730).
- Ferrando, P., Raviart, A., Haasbroek, L.J., et al., 1996. Latitude variations of $\approx 7\text{MeV}$ and $>300\text{MeV}$ cosmic ray electron fluxes in the heliosphere: ULYSSES COSPIN/KET results and implications. *Astron. Astrophys.* 316, 528–537.
- Ferreira, S.E.S., Potgieter, M.S., 2004. Long-Term Cosmic-Ray Modulation in the Heliosphere. *Astrophys. J.* 603, 744–752. doi:[10.1086/381649](https://doi.org/10.1086/381649).
- Fränz, M., Harper, D., 2002. Heliospheric coordinate systems. *Plan.Space Sci.* 50, 217–233. doi:[10.1016/S0032-0633\(01\)00119-2](https://doi.org/10.1016/S0032-0633(01)00119-2).
- Fränz, M., Harper, D., 2017. Heliospheric coordinate systems - Corrected Version. URL: <https://www2.mps.mpg.de/homes/fraenz/systems/systems3art.pdf>. [Online; accessed 16-January-2019].
- Frisch, P.C., Berdyugin, A., Piirola, V., Magalhaes, A.M., Seriacopi, D.B., Wiktorowicz, S.J., Andersson, B.G., Funsten, H.O., McComas, D.J., Schwadron, N.A., Slavin, J.D., Hanson, A.J., Fu, C.W., 2015. Charting the Interstellar Magnetic Field causing the Interstellar Boundary Explorer (IBEX) Ribbon of Energetic Neutral Atoms. *Astrophys. J.* 814, 112. doi:[10.1088/0004-637X/814/2/112](https://doi.org/10.1088/0004-637X/814/2/112), [arXiv:1510.04679](https://arxiv.org/abs/1510.04679).
- Gervasi, M., Rancoita, P.G., Usoskin, I.G., et al., 1999. Monte-Carlo approach to Galactic Cosmic Ray propagation in the Heliosphere. *Nucl. Phys. B - Proc. Sup.* 78, 26–31. doi:[10.1016/S0920-5632\(99\)00518-6](https://doi.org/10.1016/S0920-5632(99)00518-6).
- Gieseler, J., Heber, B., 2016. Spatial gradients of GCR protons in the inner heliosphere derived from Ulysses COSPIN/KET and PAMELA measurements. *Astron. and Astrophys.* 589, A32. doi:[10.1051/0004-6361/201527972](https://doi.org/10.1051/0004-6361/201527972), [arXiv:1602.00533](https://arxiv.org/abs/1602.00533).
- Gleeson, L.J., Axford, W.I., 1968. Solar Modulation of Galactic Cosmic Rays. *Astrophys. J.* 154, 1011. doi:[10.1086/149822](https://doi.org/10.1086/149822).
- Gloeckler, G., Jokipii, J.R., 1966. Low-Energy Cosmic-Ray Modulation Related to Observed Interplanetary Magnetic Field Irregularities. *Phys. Rev. Lett.* 17, 203–207. doi:[10.1103/PhysRevLett.17.203](https://doi.org/10.1103/PhysRevLett.17.203).
- Golge, S., O'Neill, P.M., Slaba, T.C., 2015. NASA galactic cosmic radiation environment model: Badhwar - O'Neill (2014), in: *The 34th International Cosmic Ray Conference*, p. PoS(ICRC2015)180.
- Haino, S., Sanuki, T., Abe, K., et al., 2004. Measurements of primary and atmospheric cosmic-ray spectra with the BESS-TeV spectrometer. *Physics Letters B* 594, 35–46. doi:[10.1016/j.physletb.2004.05.019](https://doi.org/10.1016/j.physletb.2004.05.019), [arXiv:astro-ph/0403704](https://arxiv.org/abs/astro-ph/0403704).
- Hattingh, M., Burger, R.A., 1995. A new simulated wavy neutral sheet drift model. *Adv. Space Res.* 16, 213–216.
- Heber, B., 2011. Cosmic rays through the solar hale cycle. *Space Sci. Rev.* doi:[10.1007/s11214-011-9784-x](https://doi.org/10.1007/s11214-011-9784-x).
- Heber, B., Droege, W., Ferrando, P., et al., 1996. Spatial variation of $>40\text{MeV/n}$ nuclei fluxes observed during the ULYSSES rapid latitude scan. *Astronomy and Astrophysics* 316, 538–546.
- Heber, B., Potgieter, M.S., 2006. Cosmic rays at high heliolatitudes. *Space Science Reviews* 127, 117–194. URL: <http://dx.doi.org/10.1007/s11214-006-9085-y>, doi:[10.1007/s11214-006-9085-y](https://doi.org/10.1007/s11214-006-9085-y).
- Hoeksema, J.T., 1995. The Large-Scale Structure of the Heliospheric Current Sheet During the ULYSSES Epoch. *Space Sci. Rev.* 72, 137–148. doi:[10.1007/BF00768770](https://doi.org/10.1007/BF00768770).
- Holzer, T.E., 1989. Interaction between the solar wind and the interstellar medium. *Annu. Rev. Astron. Astrophys.* 27, 199–234. doi:[10.1146/annurev.aa.27.090189.001215](https://doi.org/10.1146/annurev.aa.27.090189.001215).
- Ibarra, A., Tran, D., Weniger, C., 2010. Decaying dark matter in light of the PAMELA and Fermi LAT data. *J. Cosmol. Astropart. P.* 1, 009. doi:[10.1088/1475-7516/2010/01/009](https://doi.org/10.1088/1475-7516/2010/01/009), [arXiv:0906.1571](https://arxiv.org/abs/0906.1571).
- Ip, W.H., Axford, W.I., 1985. Estimates of galactic cosmic ray spectra at low energies. *Astron. Astrophys.* 149, 7–10.
- Jokipii, J.R., 1966. Cosmic-Ray Propagation. I. Charged Particles in a Random Magnetic Field. *Astrophys. J.* 146, 480. doi:[10.1086/148912](https://doi.org/10.1086/148912).
- Jokipii, J.R., 1971. Propagation of cosmic rays in the solar wind. *Rev. Geoph. Space Phys.* 9, 27–87. doi:[10.1029/RG009i001p00027](https://doi.org/10.1029/RG009i001p00027).
- Jokipii, J.R., Thomas, B., 1981. Effects of drift on the transport of cosmic rays. IV - Modulation by a wavy interplanetary current sheet. *Astrophys. J.* 243, 1115–1122. doi:[10.1086/158675](https://doi.org/10.1086/158675).
- Kóta, J., 2016. The Role of Particle Drifts in the Heliosphere, in: *Journal of Physics Conference Series*, p. 012014. doi:[10.1088/1742-6596/767/1/012014](https://doi.org/10.1088/1742-6596/767/1/012014).
- Krimigis, S.M., Decker, R.B., Roelof, E.C., Hill, M.E., Armstrong, T.P., Gloeckler, G., Hamilton, D.C., Lanzerotti, L.J., 2013. Search for the exit: Voyager 1 at heliosphere's border with the galaxy. *Science* 341, 144–147. URL: <http://science.sciencemag.org/content/341/6142/144>, doi:[10.1126/science.1235721](https://doi.org/10.1126/science.1235721).
- Krimigis, S.M., Mitchell, D.G., Roelof, E.C., Hsieh, K.C., McComas, D.J., 2009. Imaging the Interaction of the Heliosphere with the Interstellar Medium from Saturn with Cassini. *Science* 326, 971. doi:[10.1126/science.1181079](https://doi.org/10.1126/science.1181079).
- Kühl, P., Gómez-Herrero, R., Heber, B., 2016. Annual Cosmic Ray Spectra from 250 MeV up to 1.6 GeV from 1995 - 2014 Measured with the Electron Proton Helium Instrument onboard SOHO. *Sol. Phys.* 291, 965–974. doi:[10.1007/s11207-016-0879-0](https://doi.org/10.1007/s11207-016-0879-0), [arXiv:1603.00676](https://arxiv.org/abs/1603.00676).
- Kuznetsov, N.V., Popova, H., Panasyuk, M.I., 2017. Empirical model of long-time variations of galactic cosmic ray particle fluxes. *Journal of Geophysical Research (Space Physics)* 122, 1463–1472. doi:[10.1002/2016JA022920](https://doi.org/10.1002/2016JA022920).
- Laitinen, T., Kopp, A., Effenberger, F., Dalla, S., Marsh, M.S., 2016. Solar energetic particle access to distant longitudes through turbulent field-line meandering. *Astron. Astrophys.* 591, A18. doi:[10.1051/0004-6361/201527801](https://doi.org/10.1051/0004-6361/201527801), [arXiv:1508.03164](https://arxiv.org/abs/1508.03164).
- Landau, L.D., Lifshitz, E.M., 1959. Fluid mechanics.
- Langner, U.W., Potgieter, M.S., Webber, W.R., 2003. Modulation of cosmic ray protons in the heliosheath. *Journal of Geophysical Research (Space Physics)* 108, 8039. doi:[10.1029/2003JA009934](https://doi.org/10.1029/2003JA009934).
- Leroy, C., Rancoita, P., 2007. Particle interaction and displacement damage in silicon devices operated in radiation environments. *Reports on Progress in Physics* 70, 493. URL: <http://stacks.iop.org/0034-4885/70/i=4/a=R01>.
- Leroy, C., Rancoita, P.G., 2015. Principles of Radiation Interaction in Matter and Detection, 4th Edition. World Scientific Publishing Co.(Singapore).
- Masi, N., 2016. AMS-02 measurements interpretation: implications for dark matter indirect search, p. 282. doi:[10.1393/ncc/i2016-16282-1](https://doi.org/10.1393/ncc/i2016-16282-1).
- McComas, D.J., Allegrini, F., Bochsler, P., Bzowski, M., Christian, E.R., Crew, G.B., DeMajistre, R., Fahr, H., Fichtner, H., Frisch, P.C., Funsten, H.O., Fuselier, S.A., Gloeckler, G., Gruntman, M., Heerikhuisen, J., Izmodenov, V., Janzen, P., Knap-

- penberger, P., Krimigis, S., Kucharek, H., Lee, M., Livadiotis, G., Livi, S., MacDowall, R.J., Mitchell, D., Möbius, E., Moore, T., Pogorelov, N.V., Reisenfeld, D., Roelof, E., Saul, L., Schwadron, N.A., Valek, P.W., Vanderspek, R., Wurz, P., Zank, G.P., 2009. Global Observations of the Interstellar Interaction from the Interstellar Boundary Explorer (IBEX). *Science* 326, 959. doi:[10.1126/science.1180906](https://doi.org/10.1126/science.1180906).
- McDonald, F.B., Lal, N., 1986. Variations of galactic cosmic rays with heliolatitude in the outer heliosphere. *Geoph. Res. Lett.* 13, 781–784. doi:[10.1029/GL013i008p00781](https://doi.org/10.1029/GL013i008p00781).
- Menn, W., Hof, M., Reimer, O., Simon, M., et al., 2000. The Absolute Flux of Protons and Helium at the Top of the Atmosphere Using IMAX. *Astrophys. J.* 533, 281–297. doi:[10.1086/308645](https://doi.org/10.1086/308645).
- Mertsch, P., Sarkar, S., 2011. The 'PAMELA anomaly' indicates a nearby cosmic ray accelerator, in: Giani, S., Leroy, C., Rancoita, P.G. (Eds.), *Cosmic Rays for Particle and Astroparticle Physics*, pp. 535–543. doi:[10.1142/9789814329033_0066](https://doi.org/10.1142/9789814329033_0066), [arXiv:1108.1753](https://arxiv.org/abs/1108.1753).
- Minnie, J., Bieber, J.W., Matthaeus, W.H., et al., 2007. Suppression of Particle Drifts by Turbulence. *Astrophys. J.* 670, 1149–1158. doi:[10.1086/522026](https://doi.org/10.1086/522026).
- Möbius, E., Bzowski, M., Chalov, S., Fahr, H.-J., Gloeckler, G., Izmodenov, V., Kallenbach, R., Lallement, R., McMullin, D., Noda, H., Oka, M., Pauluhn, A., Raymond, J., Ruciński, D., Skoug, R., Terasawa, T., Thompson, W., Vallerger, J., von Steiger, R., Witte, M., 2004. Synopsis of the interstellar he parameters from combined neutral gas, pickup ion and uv scattering observations and related consequences. *A&A* 426, 897–907. URL: <https://doi.org/10.1051/0004-6361/20035834>, doi:[10.1051/0004-6361/20035834](https://doi.org/10.1051/0004-6361/20035834).
- Moloto, K.D., Engelbrecht, N.E., Burger, R.A., 2018. A Simplified Ab Initio Cosmic-ray Modulation Model with Simulated Time Dependence and Predictive Capability. *Astrophys. J.* 859, 107. doi:[10.3847/1538-4357/aac174](https://doi.org/10.3847/1538-4357/aac174).
- Moskalenko, I.V., Strong, A.W., 1998. Production and Propagation of Cosmic-Ray Positrons and Electrons. *Astrophys. J.* 493, 694–707. doi:[10.1086/305152](https://doi.org/10.1086/305152), [arXiv:astro-ph/9710124](https://arxiv.org/abs/astro-ph/9710124).
- Müller-Mellin, R., Kunow, H., Fleißner, V., Pehlke, E., Rode, E., Röschmann, N., Scharnberg, C., Sierks, H., Rusznayak, P., McKenna-Lawlor, S., Elenndt, I., Sequeiros, J., Meziat, D., Sanchez, S., Medina, J., Del Peral, L., Witte, M., Marsden, R., Henrion, J., 1995. COSTEP - Comprehensive Suprathermal and Energetic Particle Analyser. *Sol. Phys.* 162, 483–504. doi:[10.1007/BF00733437](https://doi.org/10.1007/BF00733437).
- NASA-OMNIweb, 2018. online database <http://omniweb.gsfc.nasa.gov/form/dx1.html>.
- NASA-Voyager, 2018. online database <https://voyager.gsfc.nasa.gov/flux.html>.
- NASA's Voyager team, 2018. Nasa's voyager 2 probe enters interstellar space. URL: https://voyager.jpl.nasa.gov/news/details.php?article_id=112. [Online; accessed 16-January-2019].
- Opher, M., Drake, J.F., Swisdak, M., Zieger, B., Toth, G., 2017. The Twist of the Draped Interstellar Magnetic Field Ahead of the Heliopause: A Magnetic Reconnection Driven Rotational Discontinuity. *Astrophys. J. Letter* 839, L12. doi:[10.3847/2041-8213/aa692f](https://doi.org/10.3847/2041-8213/aa692f), [arXiv:1702.06178](https://arxiv.org/abs/1702.06178).
- Opher, M., Drake, J.F., Zieger, B., Gombosi, T.I., 2015. Magnetized Jets Driven By the Sun: the Structure of the Heliosphere Revisited. *Astrophys. J. Letter* 800, L28. doi:[10.1088/2041-8205/800/2/L28](https://doi.org/10.1088/2041-8205/800/2/L28), [arXiv:1412.7687](https://arxiv.org/abs/1412.7687).
- Palmer, I.D., 1982. Transport coefficients of low-energy cosmic rays in interplanetary space. *Rev. Geophys. Space Ge.* 20, 335–351. doi:[10.1029/RG020i002p00335](https://doi.org/10.1029/RG020i002p00335).
- Parker, E.N., 1958. Dynamics of the Interplanetary Gas and Magnetic Fields. *Astrophys. J.* 128, 664. doi:[10.1086/146579](https://doi.org/10.1086/146579).
- Parker, E.N., 1961. The Stellar-Wind Regions. *Astrophys. J.* 134, 20. doi:[10.1086/147124](https://doi.org/10.1086/147124).
- Parker, E.N., 1963. Interplanetary dynamical processes.
- Parker, E.N., 1965. The passage of energetic charged particles through interplanetary space. *Plan. Space Sci.* 13, 9–49. doi:[10.1016/0032-0633\(65\)90131-5](https://doi.org/10.1016/0032-0633(65)90131-5).
- Perko, J.S., 1987. Solar modulation of galactic antiprotons. *Astron. and Astrophys.* 184, 119–121.
- Potgieter, M.S., 2000. Heliospheric modulation of cosmic ray protons: Role of enhanced perpendicular diffusion during periods of minimum solar modulation. *J. Geophys. Res.* 105, 18295–18304. doi:[10.1029/1999JA000434](https://doi.org/10.1029/1999JA000434).
- Potgieter, M.S., Le Roux, J.A., 1994. The Long-Term Heliospheric Modulation of Galactic Cosmic Rays according to a Time-dependent Drift Model with Merged Interaction Regions. *Astrophys. J.* 423, 817. doi:[10.1086/173860](https://doi.org/10.1086/173860).
- Potgieter, M.S., Moraal, H., 1985. A drift model for the modulation of galactic cosmic rays. *Astrophys. J.* 294, 425–440. doi:[10.1086/163309](https://doi.org/10.1086/163309).
- Potgieter, M.S., Mwiinga, N., Ferreira, S.E.S., Manuel, R., Ndiitwani, D.C., 2013. The long-term variability of cosmic ray protons in the heliosphere: A modeling approach. *Journal of Advanced Research* 4, 259–263. doi:[10.1016/j.jare.2012.08.001](https://doi.org/10.1016/j.jare.2012.08.001).
- Putze, A., Derome, L., Maurin, D., et al., 2009. A Markov Chain Monte Carlo technique to sample transport and source parameters of Galactic cosmic rays. I. Method and results for the Leaky-Box model. *Astron. Astrophys.* 497, 991–1007. doi:[10.1051/0004-6361/200810824](https://doi.org/10.1051/0004-6361/200810824), [arXiv:0808.2437](https://arxiv.org/abs/0808.2437).
- Raath, J.L., Potgieter, M.S., Strauss, R.D., et al., 2016. The effects of magnetic field modifications on the solar modulation of cosmic rays with a SDE-based model. *Adv. Space Res.* 57, 1965–1977. doi:[10.1016/j.asr.2016.01.017](https://doi.org/10.1016/j.asr.2016.01.017), [arXiv:1506.07305](https://arxiv.org/abs/1506.07305).
- Richardson, J.D., 2013. Voyager observations of the interaction of the heliosphere with the interstellar medium. *Journal of Advanced Research* 4, 229–233. doi:[10.1016/j.jare.2012.09.002](https://doi.org/10.1016/j.jare.2012.09.002).
- Richardson, J.D., Decker, R.B., 2015. Plasma and flows in the heliosheath. *Journal of Physics: Conference Series* 577, 012021. URL: <http://stacks.iop.org/1742-6596/577/i=1/a=012021>.
- Richardson, J.D., Kasper, J.C., Wang, C., Belcher, J.W., Lazarus, A.J., 2008. Cool heliosheath plasma and deceleration of the upstream solar wind at the termination shock. *Nature* 454, 63–66. doi:[10.1038/nature07024](https://doi.org/10.1038/nature07024).
- Rozza, D., Della Torre, S., Gervasi, M., et al., 2015. Vela-X as main contributor to the electron and positron spectra at energy above 100 GeV, in: *The 34th International Cosmic Ray Conference*, p. PoS(ICRC2015)501.
- Salati, P., 2011. Charged Cosmic Rays from Dark Matter, in: Giani, S., Leroy, C., Rancoita, P.G. (Eds.), *Cosmic Rays for Particle and Astroparticle Physics*, pp. 613–625. doi:[10.1142/9789814329033_0076](https://doi.org/10.1142/9789814329033_0076).
- Scherer, K., Fichtner, H., Strauss, R.D., et al., 2011. On Cosmic Ray Modulation beyond the Heliopause: Where is the Modulation Boundary? *Astrophys. J.* 735, 128. doi:[10.1088/0004-637X/735/2/128](https://doi.org/10.1088/0004-637X/735/2/128).
- Shalchi, A., 2009. Nonlinear Cosmic Ray Diffusion Theories. Springer-Verlag Berlin Heidelberg. doi:[10.1007/978-3-642-00309-7](https://doi.org/10.1007/978-3-642-00309-7).
- Shikaze, Y., Haino, S., Abe, K., et al., 2007. Measurements of 0.2–20 GeV/n cosmic-ray proton and helium spectra from 1997 through 2002 with the BESS spectrometer. *Astroparticle Physics* 28, 154–167. doi:[10.1016/j.astropartphys.2007.05.001](https://doi.org/10.1016/j.astropartphys.2007.05.001), [arXiv:astro-ph/0611388](https://arxiv.org/abs/astro-ph/0611388).
- Simpson, J.A., Anglin, J.D., Balogh, A., et al., 1992. The ULYSSES Cosmic Ray and Solar Particle Investigation. *Astronomy and Astrophysics Supplement Series* 92, 365–399.
- Simpson, J.A., Zhang, M., Bame, S., 1996. A solar polar north-south asymmetry for cosmic-ray propagation in the heliosphere: The Ulysses pole-to-pole rapid transit. *The Astrophysical Journal Letters* 465, L69. URL: <http://stacks.iop.org/1538-4357/465/i=1/a=L69>.
- Slavin, J. D., Frisch, P. C., 2008. The boundary conditions of the heliosphere: photoionization models constrained by interstellar and in situ data. *A&A* 491, 53–68. URL: <https://doi.org/10.1051/0004-6361/20078101>, doi:[10.1051/0004-6361/20078101](https://doi.org/10.1051/0004-6361/20078101).
- Stone, E.C., Cummings, A.C., McDonald, F.B., Heikkilä, B.C., Lal,

- N., Webber, W.R., 2005. Voyager 1 explores the termination shock region and the heliosheath beyond. *Science* 309, 2017–2020. URL: <http://science.sciencemag.org/content/309/5743/2017>, doi:10.1126/science.1117684.
- Stone, E.C., Cummings, A.C., McDonald, F.B., Heikkilä, B.C., Lal, N., Webber, W.R., 2013. Voyager 1 observes low-energy galactic cosmic rays in a region depleted of heliospheric ions. *Science* 341, 150–153. URL: <http://science.sciencemag.org/content/341/6142/150>, doi:10.1126/science.1236408.
- Strauss, R.D., Potgieter, M.S., Büsching, I., et al., 2011. Modeling the Modulation of Galactic and Jovian Electrons by Stochastic Processes. *Astrophys. J.* 735, 83. doi:10.1088/0004-637X/735/2/83.
- Strong, A.W., Moskalenko, I.V., 1998. Propagation of Cosmic-Ray Nucleons in the Galaxy. *Astrophys. J.* 509, 212–228. doi:10.1086/306470, [arXiv:astro-ph/9807150](https://arxiv.org/abs/astro-ph/9807150).
- Strong, A.W., Moskalenko, I.V., Ptuskin, V.S., 2007. Cosmic-Ray Propagation and Interactions in the Galaxy. *Annual Review of Nuclear and Particle Science* 57, 285–327. doi:10.1146/annurev.nucl.57.090506.123011, [arXiv:astro-ph/0701517](https://arxiv.org/abs/astro-ph/0701517).
- Suess, S.T., 1990. The heliopause. *Reviews of Geophysics* 28, 97–115. doi:10.1029/RG028i001p00097.
- UFA, 2018. Ulysses online final archive <http://ufa.esac.esa.int/ufa>.
- Venkatesan, D., Badruddin, 1990. Cosmic-ray intensity variations in the 3-dimensional heliosphere. *Space Sci. Rev.* 52, 121–194. doi:10.1007/BF00704241.
- Webber, W.R., McDonald, F.B., 2013. Recent Voyager 1 data indicate that on 25 August 2012 at a distance of 121.7 AU from the Sun, sudden and unprecedented intensity changes were observed in anomalous and galactic cosmic rays. *Geoph. Res. Lett.* 40, 1665–1668. doi:10.1002/grl.50383.
- Webber, W.R., Yushak, S.M., 1983. A measurement of the energy spectra and relative abundance of the cosmic-ray H and He isotopes over a broad energy range. *Astrophys. J.* 275, 391–404. doi:10.1086/161541.
- Weniger, C., 2011. Gamma-ray anisotropies from decaying dark matter. *WORLD SCIENTIFIC*. pp. 632–640. doi:10.1142/9789814329033_0078.
- World Data Center SILSO, Royal Observatory of Belgium, B., 1964–2015. The international sunspot number. *International Sunspot Number Monthly Bulletin and online catalogue*.
- WSO, 2018. Wilcox Solar Observatory; <http://wso.stanford.edu/>.
- Zank, G., 2015. Faltering steps into the galaxy: The boundary regions of the heliosphere. *Annual Review of Astronomy and Astrophysics* 53, 449–500. URL: <https://doi.org/10.1146/annurev-astro-082214-122254>, doi:10.1146/annurev-astro-082214-122254.
- Zank, G.P., 1999. Interaction of the solar wind with the local interstellar medium: a theoretical perspective. *Space Sci. Rev.* 89, 413–688. doi:10.1023/A:1005155601277.
- Zeldovich, M.A., Logachev, Y.I., Kecskeméty, K., 2005. Radial Gradients of the Low-Energy Proton Background Between 20 and 80 AU. *International Journal of Modern Physics A* 20, 6727–6729. doi:10.1142/S0217751X05029940.
- Zhang, M., Luo, X., Pogorelov, N., 2015. Where is the cosmic-ray modulation boundary of the heliosphere? *Physics of Plasmas* 22, 091501. doi:10.1063/1.4928945.
- Zirnstein, E.J., Heerikhuisen, J., Funsten, H.O., Livadiotis, G., McComas, D.J., Pogorelov, N.V., 2016. Local Interstellar Magnetic Field Determined from the Interstellar Boundary Explorer Ribbon. *Astrophys. J. Letter* 818, L18. doi:10.3847/2041-8205/818/1/L18.